



**IMPROVEMENT OF EJECTOR PERFORMANCE  
BY USING TWO STAGE EJECTOR PRINCIPLE**

**NAT SUVARNAKUTA**

**A THESIS SUBMITTED IN PARTIAL FULFILLMENT OF THE  
REQUIREMENTS FOR THE DEGREE OF DOCTOR OF PHILOSOPHY  
MAJOR IN MECHANICAL ENGINEERING  
FACULTY OF ENGINEERING  
UBON RATCHATHANI UNIVERSITY  
ACADEMIC YEAR 2019  
COPYRIGHT OF UBON RATCHATHANI UNIVERSITY**

## ACKNOWLEDGEMENTS

I would like to express my sincere appreciation to Associate Professor Dr.Kunlachate Pianthong for his supervision, suggestion, help, and support all aspects throughout this Doctoral course. His support is greatly appreciated and has been an invaluable contribution to this work. His suggestion will encourage and continuously inspiration for my future career. I would like to acknowledge Associate Professor Dr.Thanarath Sriveerakul, Associate Professor Dr.Wirapan Sehanam from Ubon Ratchathani University, and Associate Professor Dr.Chatchai Benjapiyaporn from Khon Kaen University for serving on my dissertation committee, their valuable time, helpful guidance of this Ph.D. I wish to thank the Department of Mechanical Engineering, Ubon Ratchathani University, for providing the research facilities.

Finally, I would like to thank my parents and my brother for their support in my journey to finish my Ph.D. degree. To all of you and those, I may forget, Thank you very much.

Nat Suvarnakuta  
Researcher

## บทคัดย่อ

เรื่อง : การเพิ่มสมรรถนะของอีเจ็คเตอร์ โดยใช้หลักการของอีเจ็คเตอร์แบบสองลำดับ  
 ผู้วิจัย : ญัฐ สุวรรณภูมิ  
 ชื่อปริญญา : ปรัชญาคุณภูมิบัณฑิต  
 สาขาวิชา : วิศวกรรมเครื่องกล  
 อาจารย์ที่ปรึกษา : รองศาสตราจารย์ ดร.กุลเชษฐ์ เพียรทอง  
 คำสำคัญ : อีเจ็คเตอร์แบบสองลำดับ, ระบบทำความเย็นแบบอีเจ็คเตอร์, พลศาสตร์ของไหลเชิงคำนวณ

การศึกษานี้มีวัตถุประสงค์เพื่อตรวจสอบการนำอีเจ็คเตอร์แบบสองลำดับมาใช้ในการเพิ่มสมรรถนะการทำงานของระบบทำความเย็นแบบอีเจ็คเตอร์และการใช้อีเจ็คเตอร์ในงานก๊าซ โดยผลที่ได้จากวิธีพลศาสตร์ของไหลเชิงคำนวณ (CFD) จะเปรียบเทียบความถูกต้องกับผลของชุดอุปกรณ์ทดลอง ซึ่งในระบบทำความเย็นแบบอีเจ็คเตอร์และอีเจ็คเตอร์ในงานก๊าซ มีสองคุณลักษณะที่บ่งบอกถึงสมรรถนะการทำงานของอีเจ็คเตอร์คือ อัตราส่วนการเหนี่ยวนำ (Rm) และความดันวิกฤติ (CBP)

ในระบบการทำความเย็นแบบอีเจ็คเตอร์ วิธีพลศาสตร์ของไหลเชิงคำนวณจะใช้ตรวจสอบสมรรถนะเพื่อเพิ่มความยืดหยุ่นในการทำงานและค่าสัมประสิทธิ์สมรรถนะของเครื่องทำความเย็น (COP) ซึ่งแบบจำลองการไหล 2 มิติ ที่สมมาตรรอบแกนของอีเจ็คเตอร์แบบสองลำดับ (TSE) ที่ได้พัฒนาขึ้นจะใช้เปรียบเทียบสมรรถนะการทำงานกับอีเจ็คเตอร์แบบทั่วไป (SSE) โดยมีแบบจำลองความปั่นป่วนของการไหลเป็นแบบ The shear-stress-transportation  $k-\omega$  ( $k-\omega$ -sst) ในการจำลองการไหลของอีเจ็คเตอร์แบบสองลำดับในระบบทำความเย็นนั้น ถูกวิเคราะห์สมรรถนะการทำงานที่อุณหภูมิปฐมภูมิระหว่าง 100 - 130 °C และอุณหภูมิทุติยภูมิระหว่าง 0 - 15 °C โดยผลที่ได้จากวิธีพลศาสตร์ของไหลเชิงคำนวณพบว่า อีเจ็คเตอร์แบบสองลำดับสามารถเพิ่มค่าสมรรถนะการเหนี่ยวนำได้สูงสุดร้อยละ 77.2 ในขณะที่ค่าความดันวิกฤติลดลงเล็กน้อยมีค่าสูงสุดร้อยละ 21.9 ดังนั้นจึงสามารถสรุปได้ว่าอีเจ็คเตอร์แบบสองลำดับมีความสำคัญต่อระบบทำความเย็นอย่างมีนัยสำคัญ เมื่อต้องการความสามารถในการทำความเย็นที่สูงในขณะที่ความดันของเครื่องควบแน่นต่ำ

นอกจากนี้การศึกษสมรรถนะการทำงานของอีเจ็คเตอร์แบบสองลำดับในงานก๊าซ เมื่อเปรียบเทียบกับอีเจ็คเตอร์แบบทั่วไปโดยใช้วิธีพลศาสตร์ของไหลเชิงคำนวณพบว่า เมื่ออีเจ็คเตอร์มีสภาวะการทำงานที่ความดันปฐมภูมิเท่ากับ 4 บาร์ และความดันทุติยภูมิเท่ากับ 1 บาร์ อีเจ็คเตอร์แบบสองลำดับจะมีค่าอัตราส่วนการเหนี่ยวนำลดลงเล็กน้อยร้อยละ 3.73 แต่จะมีค่าความดันวิกฤติที่เพิ่มสูงขึ้นร้อยละ 35.92 ซึ่งผลของการทำนายสมรรถนะการทำงานด้วยวิธีพลศาสตร์ของไหลเชิงคำนวณมีความสอดคล้องกับผลที่ได้จากชุดอุปกรณ์ทดลอง โดยมีค่าความคลาดเคลื่อนของอัตราส่วนการเหนี่ยวนำและค่าความดันวิกฤติร้อยละ 18.54 และ 2.00 ตามลำดับ

สรุปได้ว่า อีเจ็คเตอร์แบบสองลำดับมีความสามารถในการเพิ่มค่าความดันวิกฤติ และยังสามารถเพิ่มสมรรถนะการทำงานของอีเจ็คเตอร์จากอัตราส่วนการเหนี่ยวนำในช่วงที่มีการไหลคงที่ การศึกษาในครั้งนี้จึงสามารถนำไปสู่ความก้าวหน้าในงานด้านการทำความเย็นแบบอีเจ็คเตอร์ได้

## ABSTRACT

TITLE : IMPROVEMENT OF EJECTOR PERFORMANCE  
BY USING TWO STAGE EJECTOR PRINCIPLE

AUTHOR : NAT SUVARNAKUTA

DEGREE : DOCTOR OF PHILOSOPHY

MAJOR : MECHANICAL ENGINEERING

ADVISOR : ASSOC. PROF. KULACHATE PIANTHONG, Ph.D.

KEYWORDS : TWO-STAGE EJECTOR, EJECTOR REFRIGERATION  
SYSTEM, COMPUTATIONAL FLUID DYNAMICS

This study aims to investigate the use of the two-stage ejector to improve the ejector performance of the refrigeration system and gas/gas ejector application. The computational fluid dynamics (CFD) results were validated with the experimental values. The ejector refrigeration system and gas/gas ejector application, the two most significant parameters used to describe the performance of an ejector, were specified in terms of entrainment ratio ( $R_m$ ) and critical back pressure (CBP).

In the ejector refrigeration system, the CFD was used to investigate the performance to increase operational flexibility and COP. A 2D-axisymmetric model of a two-stage ejector (TSE) was developed and its performance was compared to that of the commonly used single-stage ejector (SSE). The shear-stress-transportation  $k-\omega$  ( $k-\omega$ -sst) model was applied as a turbulence model. The simulation of the TSE in the refrigeration system was analysed for performance using generator temperatures between 100 and 130 °C and evaporator temperatures between 0 and 15 °C. The CFD simulation results showed that the TSE provided high entrainment ratios up to 77.2%, while showing a marginal decrease in the critical back pressure up to a maximum value of 21.9%. Therefore, it can be concluded that the TSE can significantly benefit refrigeration systems requiring high refrigerating capacity while maintaining a slightly low condensing pressure.

Furthermore, the study of the TSE performance in the gas/gas ejector system compared with the SSE simulations using CFD shows that when the primary inlet pressure is 4 bar, the secondary inlet pressure is 1 bar. The TSE provides a marginal

decrease entrainment ratio of 3.73% but increases critical back pressure of 35.92%. It was found that the predicted performances of the CFD simulated models agreed well with the experimental values. Average errors of the predicted entrainment ratio and the critical back pressure were 18.54% and 2.00%, respectively.

It can be concluded that the TSE increases in critical back pressure and can improve the ejector performance in terms of the entrainment ratio ( $R_m$ ) during choked flow. The findings of this study can contribute toward advances in the field of ejector refrigeration.

## CONTENTS

	PAGE
<b>ACKNOWLEDGEMENTS</b>	<b>I</b>
<b>THAI ABSTRACT</b>	<b>II</b>
<b>ENGLISH ABSTRACT</b>	<b>III</b>
<b>CONTENTS</b>	<b>V</b>
<b>LIST OF TABLES</b>	<b>VII</b>
<b>LIST OF FIGURES</b>	<b>VIII</b>
<b>CHAPTER 1 INTRODUCTION</b>	
1.1 Motivation and background	1
1.2 Objectives	2
1.3 Scope of work	2
1.4 Expected benefits	2
<b>CHAPTER 2 THEORY AND LITERATURE SURVEY</b>	
2.1 Ejector theory	4
2.2 Performance characteristics of the ejector	10
2.3 The steam jet system	11
2.4 Background of ejector	13
2.5 Multi-ejector refrigeration systems	14
2.6 Ejector applications	20
<b>CHAPTER 3 RESEARCH METHODOLOGY</b>	
3.1 Computation fluid dynamic (CFD)	22
3.2 Refrigeration system application	24
3.3 The gas/gas ejector application	27
<b>CHAPTER 4 RESULTS AND DISCUSSIONS</b>	
4.1 CFD results of ejector refrigeration system	38
4.2 CFD and experimental of gas/gas ejector system	52
<b>CHAPTER 5 CONCLUSIONS AND RECOMMENDATIONS</b>	
5.1 Conclusions	63
5.2 Recommendations	64

**CONTENTS (CONTINUED)**

	<b>PAGE</b>
<b>REFERENCES</b>	<b>65</b>
<b>APPENDICES</b>	
A CFD results for ejector refrigeration system	73
B Experimental and CFD results for the gas/gas ejector application	75
<b>VITAE</b>	<b>79</b>

**LIST OF TABLES**

<b>TABLE</b>		<b>PAGE</b>
3.1	Parameters of the single-stage ejector	24
3.2	Properties working fluid (water vapour) use in the CFD simulation	25
3.3	Properties working fluid (air) used in the CFD simulation	29
3.4	The RSM analyzed optimum solutions the SSE	30
3.5	The RSM analyzed optimum solutions the TSE	30
3.6	Parameters of the single-stage ejector in the gas/gas ejector system	35
3.7	Parameters of the two-stage ejector in the gas/gas ejector system	36
3.8	Instruments introduction	37
4.1	Validation of calculated primary mass flow rate with the experimental values.	57

## LIST OF FIGURES

<b>FIGURE</b>	<b>PAGE</b>
2.1 Configurations of typical ejector	4
2.2 Schematic representation of and ejector	6
2.3 Performance characteristics of a steam ejector	10
2.4 A schematic view of steam jet refrigeration cycle	11
2.5 Typical ejector cross section and pressure and velocity profiles	12
2.6 Two-stage ejector refrigeration system	15
2.7 Venturi tube configurations	16
2.8 Schematic and P-h diagram for ERC cycle	17
2.9 Schematic and P-h diagram for NERC cycle	17
2.10 Numerical domain of the single-stage ejector-diffuser system (SSED)	18
2.11 Numerical domain of the two-stage ejector-diffuser system (TSED)	18
2.12 Schematic of test system of supersonic natural gas ejector (TSED)	19
3.1 The single-stage ejector used in the research study	24
3.2 Geometry domain and grid structure of the single-stage ejector CFD model	27
3.3 Geometry domain and grid structure of the two-stage ejector CFD model	27
3.4 Geometry domain and grid structure of the SSE gas/gas ejector CFD model	31
3.5 Geometry domain and grid structure of the TSE gas/gas ejector type annular secondary at second stage CFD model	31
3.6 System scheme of the SSE in the gas/gas ejector system	32
3.7 The experimental SSE gas/gas ejector system	32
3.8 System scheme of the TSE in the gas/gas ejector system	33
3.9 The experimental TSE gas/gas ejector system	33

## LIST OF FIGURES (CONTINUED)

FIGURE	PAGE	
3.10	Dimensional of the primary nozzle in the gas/gas ejector system (scale : mm)	34
3.11	Photograph of the primary nozzle in the gas/gas ejector system	34
3.12	Photograph of the single-stage ejector in the gas/gas ejector system System	35
3.13	Photograph of the two-stage ejector in the gas/gas ejector system	36
4.1	Effect of the area ratio ( $A_4 / A_6$ ) in the mixing chamber geometries at the second stage on the entrainment ratio	39
4.2	Effect of length ( $L_4$ ) in the mixing chamber geometries at the second stage on the entrainment ratio	39
4.3	Effect of convergence angle ( $\theta_{II}$ ) in the mixing chamber at the second stage on the entrainment ratio	40
4.4	Comparison advantages of two-stage ejector and single-stage ejector	41
4.5	Fluid mass flow rate of SSE and TSE steam ejector at the evaporator temperature of 0 °C	42
4.6	Fluid mass flow rate of SSE and TSE steam ejector at the evaporator temperature of 5 °C	43
4.7	Fluid mass flow rate of SSE and TSE steam ejector at the evaporator temperature of 10 °C	43
4.8	Fluid mass flow rate of SSE and TSE steam ejector at the evaporator temperature of 15 °C	44
4.9	Performance characteristics of the steam ejector, effect of primary and secondary inlet temperature	45
4.10	Refrigeration capacity map	46
4.11	Demonstrates difference percentage of COP, and critical condenser pressure ( $P_{c,cri}$ ) between TSE and SSE	46
4.12	Schematic view of two-stage ejector	47

## LIST OF FIGURES (CONTINUED)

<b>FIGURE</b>	<b>PAGE</b>
4.13 Validation of secondary fluid mass flow rate of SSE, and TSE has to the check valve in the secondary fluid inlet (stage 2)	48
4.14 Secondary fluid mass flow rate of SSE and TSE steam ejector at the generator temperature of 110 °C, evaporator temperature of 0 °C	49
4.15 Secondary fluid mass flow rate of SSE and TSE steam ejector at the generator temperature of 110 °C, evaporator temperature of 15 °C	49
4.16 Secondary fluid mass flow rate of SSE and TSE steam ejector at the generator temperature of 100 °C, evaporator temperature of 10 °C	50
4.17 Secondary fluid mass flow rate of SSE and TSE steam ejector at the generator temperature of 120 °C, evaporator temperature of 10 °C	50
4.18 The Rm of SSE and TSE steam ejector at the generator temperature of 100, 110, and 120 °C, evaporator temperature of 10 °C	51
4.19 The Rm of SSE and TSE steam ejector at the generator temperature of 110 °C, evaporator temperature of 0, 10, and 15 °C	51
4.20 The Rm of SSE and TSE steam ejector at the generator temperature of 110 and 120 °C, evaporator temperature of 10 and 15 °C	52
4.21 Rm of SSE and TSE gas/gas ejector at the secondary inlet pressures are between 0.0 and 1.0 bar	53
4.22 Rm of SSE and TSE gas/gas ejector at the primary inlet pressures are between 2 and 7 bar	53
4.23 Performance characteristics of the gas/gas ejector at the primary inlet pressures is 4 bar.	54
4.24 Performance characteristics of the gas/gas ejector at the primary inlet pressures is 5 bar	54
4.25 Validation of Rm, effect of operating conditions	55
4.26 Comparison advantages of two-stage ejector and single-stage ejector in the gas/gas system	56

**LIST OF FIGURES (CONTINUED)**

<b>FIGURE</b>		<b>PAGE</b>
4.27	Validation of performance characteristics between the SSE and the TSE at $P_p = 4$ bar and $P_s = 1$ bar	58
4.28	Validation of performance characteristics between the SSE and the TSE at $P_p = 5$ bar and $P_s = 1$ bar	59
4.29	Validation of performance characteristics between the SSE and the TSE at $P_p = 5$ bar and $P_s = 0.9$ bar	59
4.30	Validation of static pressure profile along ejector between the SSE and the TSE at $P_p = 4$ bar and $P_s = 1$ bar	60
4.31	Validation of static pressure profile along ejector between the SSE and the TSE at $P_p = 5$ bar and $P_s = 1$ bar	61
4.32	Validation of static pressure profile along ejector between the SSE and the TSE at $P_p = 5$ bar and $P_s = 0.9$ bar	61

# CHAPTER 1

## INTRODUCTION

### 1.1 Motivation and background

The world energy issue is essential because the current demand for energy in various fields has been increasing steadily and rapidly. One of the most energy usages are refrigeration and air conditioning applications. Therefore, it would be useful to reduce the energy usage by, for example, efficiency improvement and ejector adaptation in the refrigeration system. An ejector is an inexpensive device that can utilize even free sources of energy like solar collector or industrial waste heat. It can replace or combine with a mechanical compressor in the refrigeration system, which is less dependent on electricity.

Various ejector refrigeration systems are described with the associated studies, and categorized as conventional ejector refrigeration system, combined refrigeration system, advanced ejector refrigeration system/Multi-components ejector refrigeration system (MERS) [1, 2]. The MERS geometric structure, such as the two-stage ejector (TSE), dramatically affects its performance. The design concept of the proposed two-stage ejector can classify into two types, which are annular primary and annular secondary, at the second stage were first invented by Grazzini in 1998. The simulation results by Grazzini show that annular primary has a high ejector compression ratio with a very compact geometrical configuration but low entrainment [3, 4] and annular secondary improves the entrainment ratio of a conventional single-stage ejector [5, 6].

Regarding the flow phenomena in an ejector, the pressure fluids known as “a primary fluid” expands and accelerates through the primary nozzle to create a supersonic speed, low-pressure fluids known as “a secondary fluid” to be entrained into the mixing chamber. Thus, increasing one more mixing chamber can increase the capability of low-pressure fluid induction, which is the two-stage ejector type annular secondary at the second stage.

The aim of this study is to investigate the performance of gas/gas ejector application utilizing the two-stage ejector (TSE) type annular secondary at the second stage by using computational fluid dynamics (CFD) and experimental methods to compare its performance with a single-stage ejector (SSE).

## **1.2 Objectives**

This thesis studies the design of the proposed two-stage ejector type annular secondary at the second stage, without changing the area ratio ( $A_r$ ) of the ejector, to investigate the performance of ejector refrigeration system and the gas/gas ejector application using the validation of the CFD and experimental results compared with those of the single-stage ejector. The two most important parameters used to analyze the performance of an ejector are the entrainment ratio ( $R_m$ ) and critical back pressure (CBP).

## **1.3 Scope of work**

1.3.1 Design of two-stage ejector (TSE) type annular secondary at the second stage in an ejector refrigeration system and the gas/gas ejector system.

1.3.2 The performance investigation using the CFD for comparing the TSE with the SSE in terms of entrainment ratio ( $R_m$ ) and critical back pressure (CBP).

1.3.3 The CFD methods and algorithms to solve and analyze the systems involving fluid flows were applied using the commercial software GAMBIT 2.3 and FLUENT 6.3.

1.3.4 The TSE refrigeration system was analyzed using generator temperatures between 100 and 130 °C and evaporator temperatures between 0 and 15 °C.

1.3.5 The TSE gas/gas ejector system was analyzed using primary inlet pressure between 4 and 5 bar and secondary inlet pressure between 0.5 and 1.0 bar.

1.3.6 The experimental results of TSE were compared with the results of SSE in the gas/gas ejector system, and validated with the CFD results.

## **1.4 Expected benefits**

This thesis expects to create the prototype of the system and particular data of two-stage ejector to improve conventional gas/gas ejector application and ejector

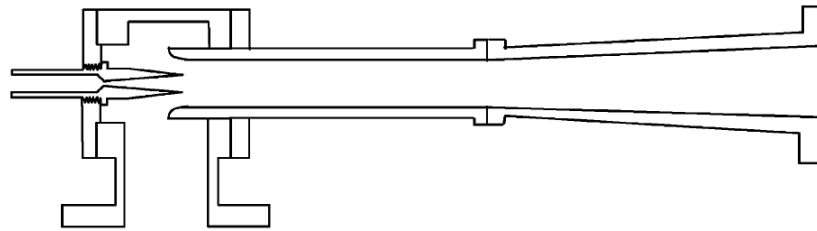
refrigeration system toward energy efficiency and reduce global warming issues. The authors expect that the information provided could contribute to the idea of improving the performance of the TSE in various applications which can also contribute to the advanced field of ejector refrigeration. Further study on experimental investigation of the TSE performance and including it in the ejector refrigeration system should be carried out.

## CHAPTER 2

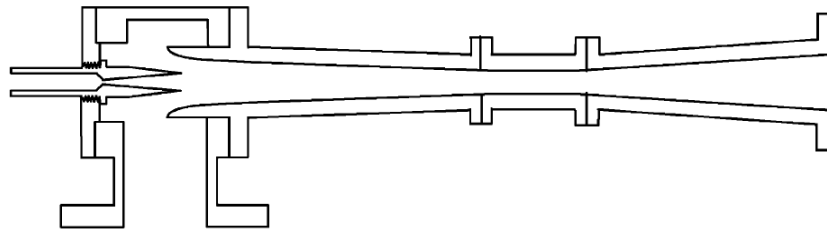
### THEORY AND LITERATURE SURVEY

#### 2.1 Ejector theory

The first application of ejector was used for removing air from the condenser of a steam engine by Sir Charles Parsons [7]. After that the ejector has developed a numerical method using one-dimensional continuity, momentum, and energy equations to investigate the ejector performance presented by Keenan and Neumann [8] it wasn't effortless to explain the mixing phenomena analytically. Therefore, their study was continued by Keenan et al. [9], who concluded that there were two types of the ejector, which has named as constant-area mixing ejector and constant-pressure mixing ejector. Two major types of ejectors shown in Figure. 2.1 [10].



(a) Constant-Area Mixing Ejector



(b) Constant-Pressure Mixing Ejector

**Figure 2.1 Configurations of typical ejector [10]**

The one-dimensional compressible flow theory could be applied to first ejector model evaluation and analysis on ideal gas dynamics as well as the principles of conservation of mass, momentum, and energy. The approached 1-D model was only provided solutions for ejectors with constant-area mixing chambers as opposed to a conical mixing section (constant-pressure mixing ejector). Later the theoretical model was extended to include a constant pressure mixing chamber and a diffuser to include irreversibility associated with the primary nozzle, mixing chamber, and diffuser [11]. The analysis of steady-state and steady flow equations commonly known as energy, momentum, and continuity can be written as following (2.1), (2.2) and (2.3).

Energy equation for an adiabatic process:

$$\sum \dot{m}_i (h_i + V_i^2 / 2) = \sum \dot{m}_o (h_o + V_o^2 / 2) \quad (2.1)$$

Momentum equation:

$$P_i A_i + \sum \dot{m}_i V_i = P_o A_o + \sum \dot{m}_o V_o \quad (2.2)$$

Continuity equation:

$$\sum \rho_i V_i A_i = \sum \rho_o V_o A_o \quad (2.3)$$

The following assumptions refer to Figure 2.2:

- (1) Isentropic efficiencies were introduced to the primary nozzle, diffuser, and mixing chamber of the ejector to account for friction losses.
- (2) The primary and secondary flows entered the ejector at zero velocity.
- (3) The primary nozzle plane (1), where the primary and secondary stream flow first met, static pressure was assumed to be uniform.
- (4) At the mixing of the primary and secondary stream flows completed before a normal shock wave occurred at the end of the mixing chamber.

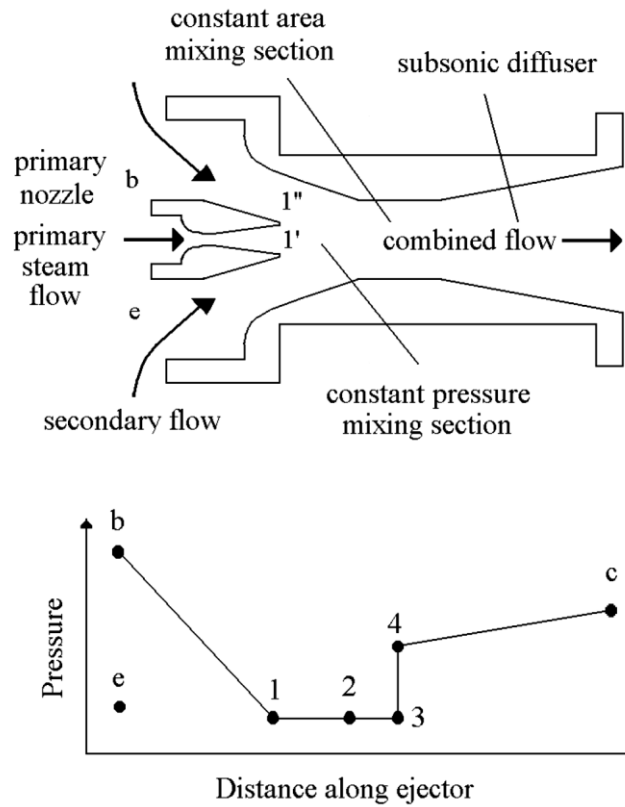


**Figure 2.2 Schematic representation of and ejector**

### 2.1.1 Mach number of the primary fluid at the nozzle exit plane

The high-pressure primary fluid at  $b$  expands through the nozzle and exits at  $1'$  with supersonic speed. If the energy equation is applied between  $b$  and  $1'$  and then simplified, the result is:

$$V_{1'}^2 = 2\eta_p(h_p - h_{1'}) \quad (2.4)$$

Where  $\eta_p$  is an isentropic efficiency of the primary nozzle. The relation between the pressure ratio across the nozzle and Mach number at the exit of the nozzle as:

$$M_{1'} = \sqrt{\frac{2\eta_p}{k-1} \left[ \left( \frac{P_p}{P_1} \right)^{\frac{k-1}{k}} - 1 \right]} \quad (2.5)$$

### 2.1.2 Mach number of the secondary fluid at the nozzle exit plane

The secondary flow expands from e to 1''. The Mach number for the secondary flow at the nozzle exit plane is derived similarly:

$$M_{1''} = \sqrt{\frac{2}{k-1} \left[ \left( \frac{P_s}{P_1} \right)^{\frac{k-1}{k}} - 1 \right]} \quad (2.6)$$

### 2.1.3 The mixing process

The momentum equation for ideal mixing is applied between 1 and 3:

$$P_1 A_1 + \dot{m}_p V_{1'} + \dot{m}_s V_{1''} = P_3 A_3 + (\dot{m}_p + \dot{m}_s) V_3 \quad (2.7)$$

Two assumptions made about the entire mixing process between primary and secondary flows occur between 1 and 3 at constant static pressure ( $P_1=P_3$ ). The cross-sectional areas at the inlet and exit of the mixing chamber are equal ( $A_1=A_3$ ). Therefore:

$$\dot{m}_p V_{1'} + \dot{m}_s V_{1''} = (\dot{m}_p + \dot{m}_s) V_3 \quad (2.8)$$

The above relation described fully idealized mixing and included as efficiency for the entire mixing chamber:

$$\eta_m (\dot{m}_p V_{1'} + \dot{m}_s V_{1''}) = (\dot{m}_p + \dot{m}_s) V_3 \quad (2.9)$$

The velocity of the mixed fluid at 3 explicitly expressed as:

$$V_3 = \eta_m \left[ \frac{\dot{m}_p V_{1'} + \dot{m}_s V_{1''}}{\dot{m}_p + \dot{m}_s} \right] \quad (2.10)$$

Equation (2.10) can be rewritten in terms of the Mach number:

$$M_3^* = \eta_m \left[ \frac{M_{1'}^* + \left( Rm \times M_{1''}^* \sqrt{\frac{T_s}{T_p}} \right)}{\sqrt{(1 + Rm) \times \left( 1 + Rm \sqrt{\frac{T_s}{T_p}} \right)}} \right] \quad (2.11)$$

The entrainment ratio (Rm) of the ejector is defined as the ratio between the evaporator (secondary) and generator (primary) fluid mass flow rates.

Where the relationship between M and  $M^*$  is given as:

$$M^* = \sqrt{\frac{(k+1) \cdot \left( \frac{M^2}{2} \right)}{1 + (k-1) \cdot \left( \frac{M^2}{2} \right)}} \quad (2.12)$$

#### 2.1.4 Pressure ratio across a normal shock wave

A normal shock wave occurs within the constant-area mixing section if the velocity of the mixing steams flow entering the section is supersonic. During the shock process, the flow experiences a sudden change in the flow velocity and pressure. Theoretically, the shock wave has an infinitesimal thickness. The shock occurring between 3 and 4 would, therefore, be an irreversible compression process in which the Mach number suddenly falls to less than unity. The Mach number of the mixed flow after the shock is:

$$M_4 = \sqrt{\frac{M_3^2 + \frac{2}{(k-1)}}{\left[ \frac{2k}{(k-1)} M_3^2 \right] - 1}} \quad (2.13)$$

The pressure lift ration across the shock wave is:

$$\frac{P_4}{P_3} = \frac{1 + kM_3^2}{1 + kM_4^2} \quad (2.14)$$

### 2.1.5 Pressure lift ratio across the subsonic diffuser

The mixed flow further compressed as it passes through the subsonic diffuser. In an additional assumption, the mixed flow velocity reduces to zero at the diffuser exit (c). The pressure lift ratio across the diffuser is:

$$\frac{P_b}{P_4} = \left[ \left( \frac{\eta_d(k-1)}{2} M_4^2 \right) + 1 \right]^{\left( \frac{k}{k-1} \right)} \quad (2.15)$$

The solutions of equations (2.4) - (2.15) were applied as follows.

The temperature, pressure, and mass flow rate of the primary and secondary fluids are all known. Temperatures and pressure derived from the thermocouples and pressure gauges. The mass flow rate calculated from the volume flow over a certain period. The following procedure used to obtain the ejector exhaust pressure.

- (1) The pressure at the nozzle exit plane is unknown and determined by an iterative process. An initial value for  $P_1/P_s$  was guessed.
- (2) Mach number of the primary and secondary fluids at the nozzle exit plane ( $M_1'$  and  $M_1''$ ) calculated from equations (2.5) and (2.6).
- (3) Mach number of the mixed fluid  $M_3$  and  $M_4$  are calculated from equation (2.11) and Equation (2.13), respectively.
- (4) The pressure lift ratio across the shock wave ( $P_4/P_3$ ) calculated from equation (2.14).
- (5) The pressure lift ratio across diffuser ( $P_c/P_4$ ) calculated from equation (2.15).
- (6)  $P_4/P_3$ ,  $P_b/P_4$ , and  $P_1/P_s$  are all known and the exhaust pressure ( $P_b$ ) can be calculated.
- (7) Steps 1 to 6 are repeated with new values of  $P_1/P_s$  until the maximum  $P_b$ .

Eames et al. suggested values of 0.85, 0.85 and 0.95 for the primary nozzle, diffuser and mixing chamber efficiencies respectively [11]. According to these authors, these values found to give an acceptable correlation with experimental data provided by ESDU [12].

## 2.2 Performance characteristics of the ejector

The most important parameters for assessing ejector performance are the entrainment ratio ( $R_m$ ), defined as the ratio of mass flow rate of the secondary flow ( $\dot{m}_s$ ) to that of the primary flow ( $\dot{m}_p$ ), and the pressure lift ratio (PLR), defined as the ratio of the ejector back pressure ( $P_b$ ) to the secondary flow pressure ( $P_s$ ).

$$R_m = \frac{\dot{m}_s}{\dot{m}_p} \quad (2.16)$$

$$PLR = \frac{P_b}{P_s} \quad (2.17)$$

The “choked flow” region is a phenomenon that occurs under specific conditions when fluid flow at a certain pressure passes through a restriction into a lower pressure and the velocity reaches to sound speed, in which the mass flow rate of the fluid becomes irrelevant to the downstream pressure. In other words, the choked flow is constant when the back pressure and even the downstream are below the critical back pressure (CBP), the primary flow and the secondary flow are both choked, causing a constant mass flow rate. As a result, the  $R_m$  stays constantly as  $P_b$  changes increase beyond CBP, entering into the “unchoked flow” region, the  $R_m$  will drop sharply due to the absence of the secondary flow choking. Further increase in  $P_b$  beyond break down pressure will lead to a “reversed flow” region or malfunction mode, where  $R_m$  is zero and, further, a reverse flow might occur is shown in Figure 2.3.

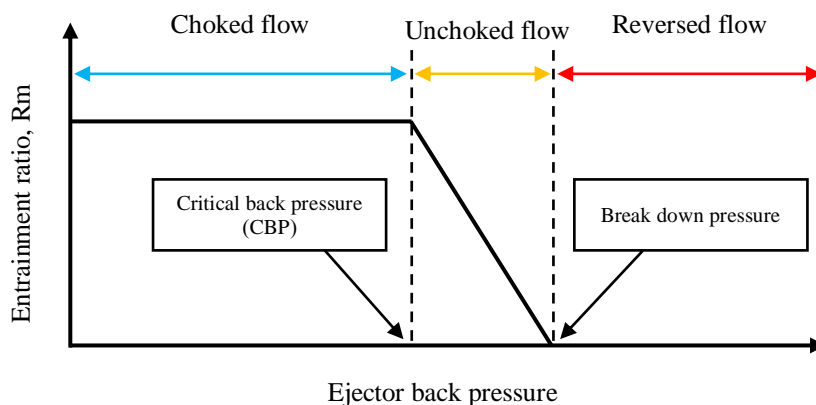


**Figure 2.3 Performance characteristics of a steam ejector**

### 2.3 The steam jet system

A steam jet refrigerator was first developed early as 1900 [13]. It experienced a wave of popularity in the air conditioning systems of buildings during the early 1930s [14]. The air conditioning system was replaced with a more favorable vapour compression system. It was superior in the coefficient of performance (COP), compactness, flexibility, and the system would become less dependent on electricity in manufacturing and operation.

The steam jet refrigeration cycle is similar to the conventional vapour compression cycle except that the compressor is replaced by a liquid feed pump, boiler/vapour-generator, and ejector-pump as shown in Figure 2.4 [15]. The system, watery liquid is vaporized at high pressure a boiler fed to an ejector where it entrains a low pressure vapour originating from the evaporator. The combined liquid flow is then compressed to an intermediate pressure equal to that of the condenser. This refrigeration cycle has drawn renewed attention due to its simplicity of construction, ruggedness and few moving parts.

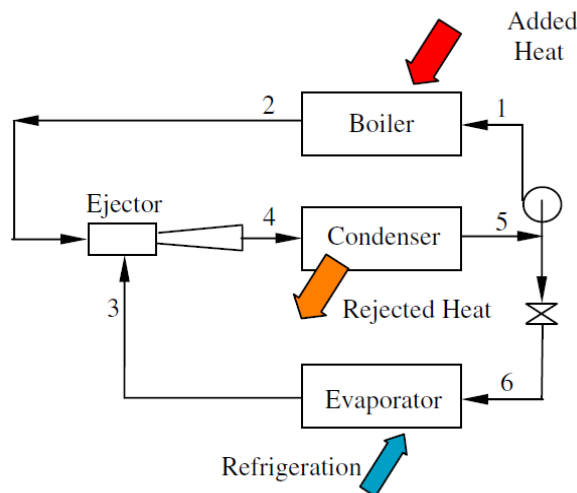


**Figure 2.4 Schematic view of steam jet refrigeration cycle [15]**

The typical ejector cross section with velocity and pressure profiles with distance along ejector is shown in Figure 2.5 [10, 15]. The primary fluid is high pressure steam expands and accelerates through the primary nozzle (i) with supersonic speed flow and creates a low pressure region at the nozzle exit plane (ii) and subsequently entrains a secondary fluid into the mixing chamber of ejector. High pressure steam of primary

fluid expanded wave flow and form a converging duct without mixing with the secondary fluid. Secondary fluid steam rises to sonic value (iii) and chokes at some cross section distance along this duct. Then the mixing fluid process begins after the secondary flow chokes, and the primary fluid flow to be retarded whilst the secondary flow is accelerated. The two steams at the end of the mixing chamber are completely mixed and the static pressure is assumed to remain constant until it reaches the throat section (iv). Mixing steam to high pressure at the mixing chamber's throat region, a normal shock of essential zero thickness is induced (v). This shock of flow causes a significant compression effect and a sudden drop in the speed from supersonic to subsonic. The mixing compression of the flow is increased (vi) until stagnated at the subsonic diffuser. In the subsonic diffuser part, the flow expands of this through a thermodynamic shock process. The shock wave causes a rise in the static pressure and its location varies with the condenser pressure. The flow from the shock wave is compressed in the diffuser and subsonic velocity to the saturation pressure of the condenser (vii).

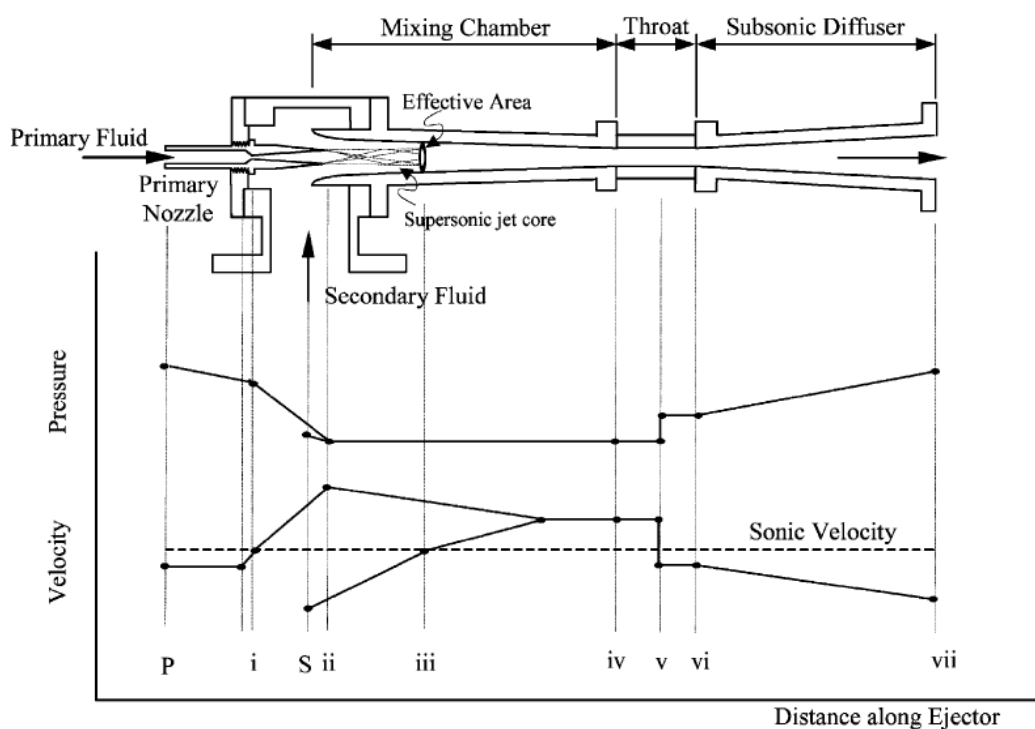


**Figure 2.5 Typical ejector cross section and pressure and velocity profiles [10]**

The operating condition of the ejector refrigeration system with a boiler/generator evaporator and the condenser are defined by a heat source, refrigeration capacity, and local climate respectively. The work input required for the circulating pump carries the heat supplied to the generator. Thus, the actual coefficient of performance (COP) of the ejector refrigeration system could be written as the following equation:

$$\text{COP} = \frac{\text{heat absorbed at the evaporator}}{\text{heat input at the generator}} \quad (2.18)$$

The COP of a steam ejector refrigeration system, which is relevant to the entrainment ratio (Rm) of the ejector, may be estimated as:

$$\text{COP} = \text{Rm} \left[ \frac{(h_{g,\text{evap}} - h_{f,\text{cond}})}{(h_{g,\text{generator}} - h_{f,\text{cond}})} \right] \quad (2.19)$$

From Equation 2.19, the ratio of the heat rejection at the evaporator to the heat input at the vapour generator/boiler observed that COP with a value of:

$$\left[ \frac{(h_{g,\text{evap}} - h_{f,\text{cond}})}{(h_{g,\text{generator}} - h_{f,\text{cond}})} \right] \quad (2.20)$$

It is almost constant for each operating condition. Thus, the performance curve of the jet refrigerator (COP) and the performance curve of the ejector (Rm) are similar.

## 2.4 Background of ejector

An ejector is well known for its versatility and diversity and has been applied in refrigeration technologies. The essential element affected the optimum performance of the ejector systems are the system conditions and ejector structures.

The system working processes with various methods have been used to study the working characteristics of the ejector refrigeration system. Mathematical simulation is a quick and straightforward way to evaluate system performance [16]. Grey system

theory provides another option for system analysis [17]. Experiments are always irreplaceable and results indicate that such systems have a high potential for extensive use [18-20].

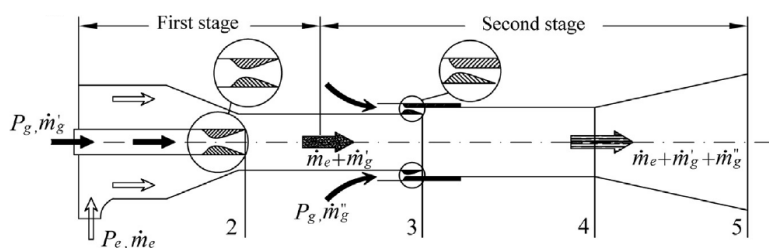
The conventional ejector refrigeration system has a relatively low COP, thereafter researchers have tried to find a more advanced ejector refrigeration system with a higher COP utilizing simulation and experiments. Attempts in this respect have been made in the following ways: changing ejector configurations, eliminating the mechanical pump, using a regenerator and/or a pre-cooler, and introducing multi-stage ejectors.

An ejector structure in terms of geometric structure considerably affects its performance. For example, the nozzle position impacts the system COP and cooling capacity [21-23], and an ejector with a spindle varying the primary throat area in the nozzle can provide a fine-tuning flexibility for its operation [24, 25]. Using a movable nozzle or adding a movable spindle is relatively easy and useful to optimize the ejector performance and improve the efficiency of the mixing process, a pressure-exchange ejector, and different nozzle structures. Altering the primary nozzle throat diameter could be compared as adjusting the area ratio ( $A_r$ ) of ejector which has a direct impact on the performance of the ejector.  $A_r$  is the ratio between the primary nozzle throat area and ejector throat area, the smallest cross-sectional area [26-28].

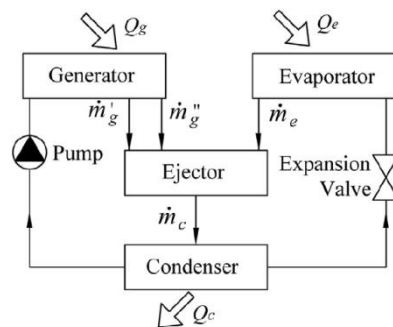
## **2.5 Multi-ejector refrigeration systems**

A multi-ejector system is difficult for a single-stage ejector to keep the system running at optimum conditions because of the critical back pressure. This motivates researchers to solve this problem by using multi-stage ejector refrigeration systems [3, 4], developing a two-stage ejector, consisting of a traditional first stage without a diffuser and an annular second stage which is directly located at the outlet of the first stage mixing chamber. Figure 2.6 schematically describes such ejector structure and whole system as well as its P-h diagram. The vapor from the generator is divided into two parts to enhance the ejector performance, both acting as the primary flow for different secondary flows in the two-stage ejector.

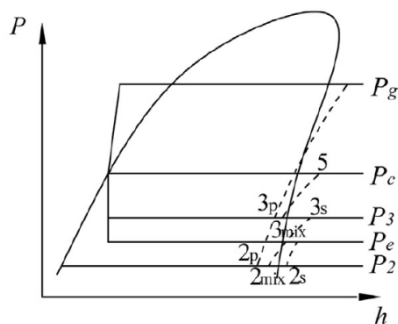
Gamisans et al. (2002: 251 - 266) [29] investigated the venturi tube performance under four different types of TSEs shown in Figure 2.7. The performance of the scrubber is varied by several factors such as gas pollutant concentration, airflow rate, and absorbing solution flow rate. The results showed a strong influence of the liquid scrubbing flow rate on pollutant removal efficiency. The increase in pressure drop strongly limits the use of two-stage venturi scrubbers, thus, the associated energy consumption.



(a) Ejector configuration



(b) System scheme



(c) P-h diagram

Figure 2.6 Two-stage ejector refrigeration system [3, 4]

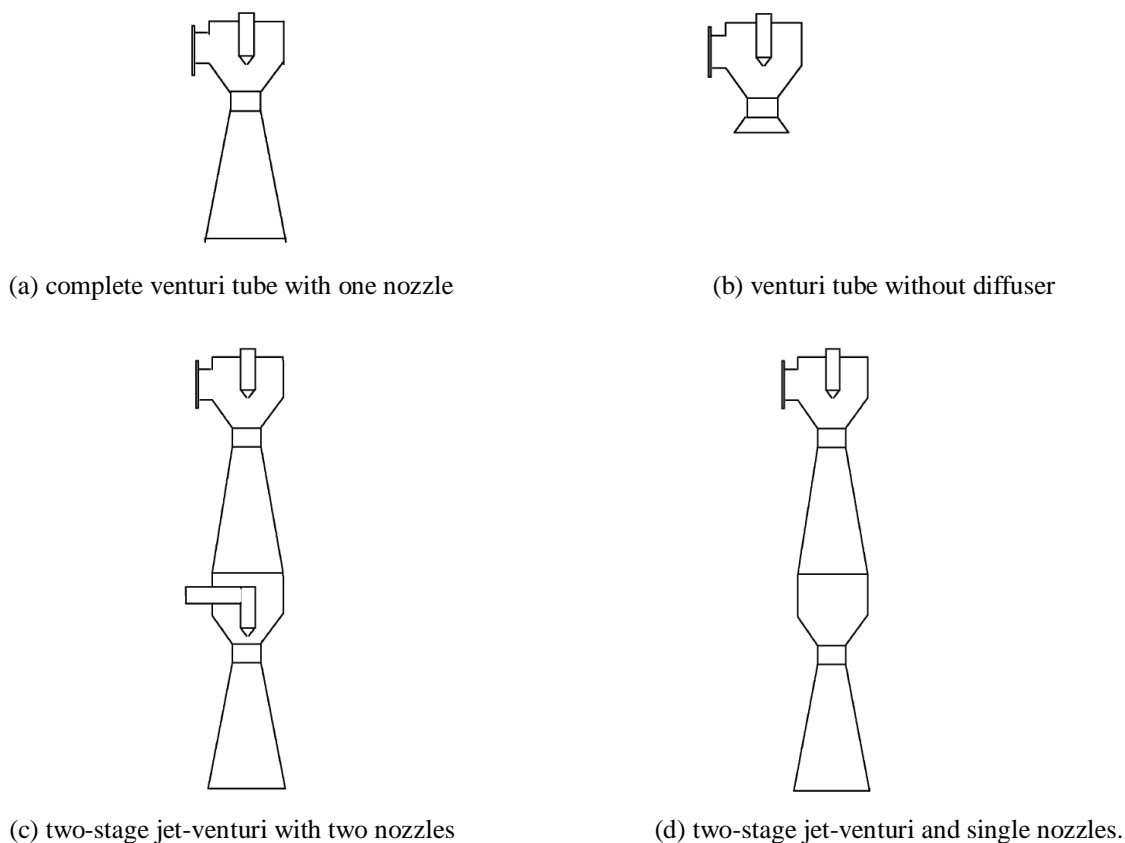


**Figure 2.7 Venturi tube configurations [29]**

Jianlin Yu et al. (2013: 166 - 172) [30] presented a theory of a new ejector enhanced vapour compression refrigeration cycle operating with the refrigerant R22. This cycle of an ejector was employed with two suction inlets to recover the expansion process losses of the cycle. Figure 2.8 shows the schematic and P-h (pressure-specific enthalpy) diagrams for a convention ejector expansion refrigeration cycle (ERC) and Figure 2.9 shows a new ejector enhanced refrigeration cycle (NERC) utilizing a two-stage suction ejector. Found that the higher pressure refrigerant saturated vapour leaving separator was used as the suction flow of the compressor to increase the suction pressure of the compressor and decrease the pressure ratio of the mechanical work of the compressor. Finally, the theoretical results indicated that the NERC can improve the cycle COP and volumetric cooling capacity or heating capacity by using a two-stage suction ejector.

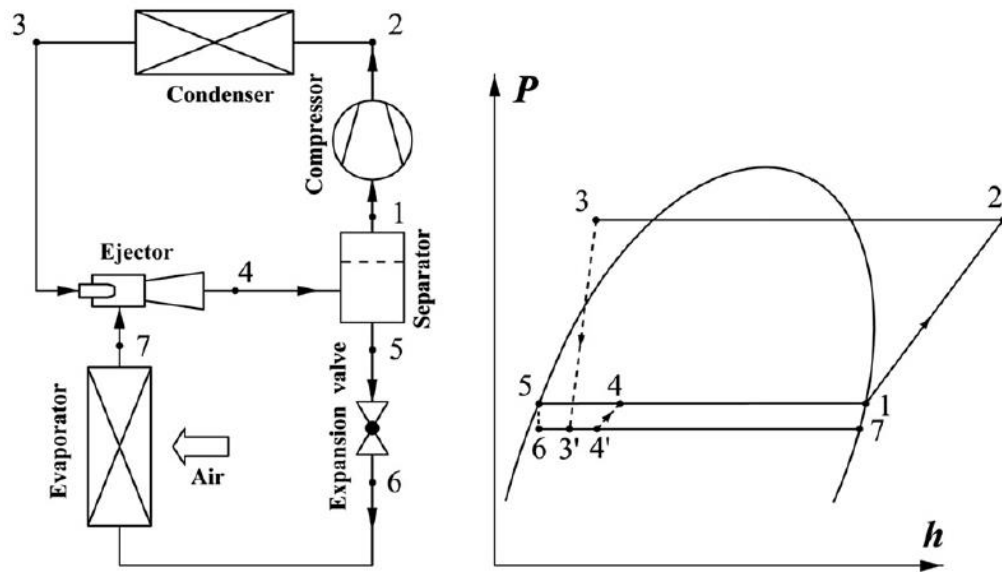


Figure 2.8 Schematic and P-h diagram for ERC cycle [30]

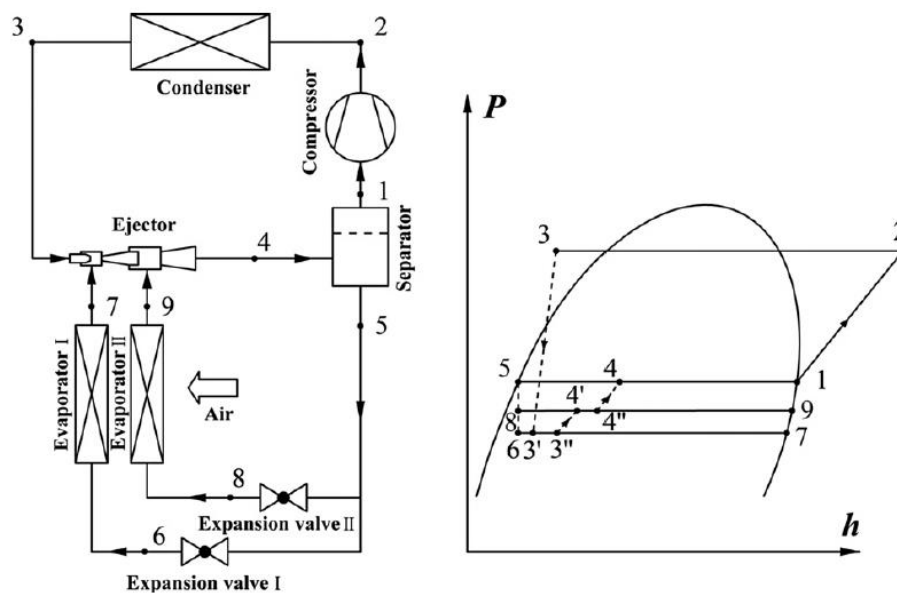
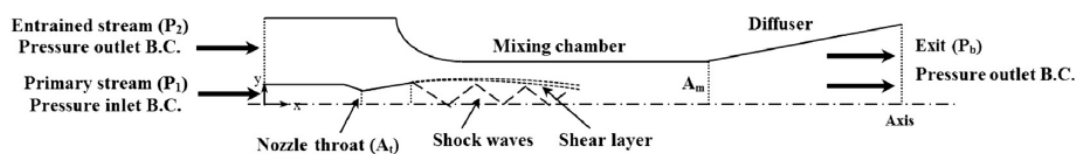


Figure 2.9 Schematic and P-h diagram for NERC cycle [30]

Kong and Kim (2013: 71 - 87) [5] studied the two-stage ejector by numerical and theoretical methods. They analyzed geometrical factors (the area ratio between the first and second stages) and operational factors (pressure ratio) on the ejector performance. The differences in the geometries and boundary conditions of the single-stage ejector-diffuser system (SSED) and the two-stage ejector-diffuser system

(TSED) illustrated in Figure 2.10 and Figure 2.11, respectively. In the SSED system, only the diffuser was removed to produce higher momentum for the second-stage ejector. The geometry of the second-stage ejector duplicated from the SSED model without the primary stream nozzle. The second diffuser was reserved to reduce the momentum loss at the exit of the second stage ejector. The pressure inlet boundary condition applied to the primary steam inlets of both models and pressure outlet boundary conditions used on all the entrained stream inlets. Adiabatic and no-slip conditions applied for wall boundaries. They mainly focused on the larger area ratio (in the range of 1-10) and the primary to back pressure ratio (ranges from 5 to 10). Furthermore, Kong and Kim [6] studied the geometrical effects of a TSED on its performance investigated with the help of a computational fluid dynamics method, and the results can be very helpful in designing the engineering TSEDs.



**Figure 2.10 Numerical domain of the single-stage ejector-diffuser system (SSED)**

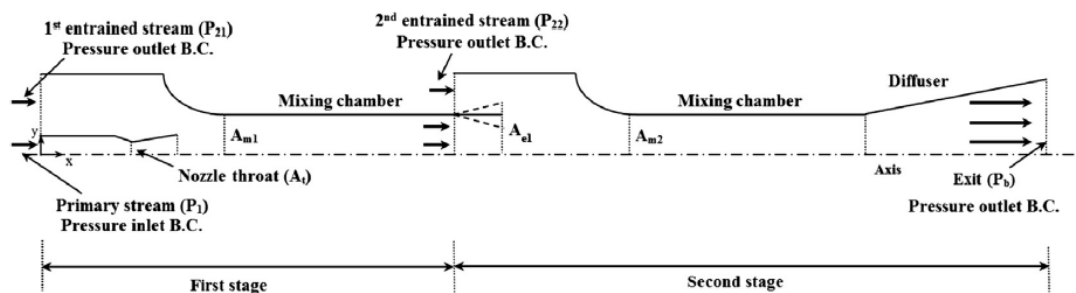


**Figure 2.11 Numerical domain of the two-stage ejector-diffuser system (TSED)**

Chen et al. (2016: 1151 - 1162) [31] studied TSE to boost low-pressure natural gas well. The ejector schematic diagram is shown in Figure 2.12. Natural gas from the high-pressure wells was first heated between 12 to 14 MPa, low-pressure between 2 to 4.5 MPa. The outlet pressure would be recompressed to the back pressure, which depends on the pipeline or transportation requirements (the value is 5.2 MPa). The performance of the ejector was analyzed through the numerical technique. The CFD

method was adopted to gain and analyze the effect of geometrical factors at the second stage, including the area ratio and length ratio. Meanwhile, the influence of the induced pressure of two induced inlets and the detailed flow field inside the ejector were analyzed through CFD visualization. As following studies, the main conclusion is that an area ratio has a significant effect on the entrainment ratio, the mixing tube length of the second stage plays an important role in the entrained capacity of TSE, and the entrainment ratio always increases as the induced pressure increases.

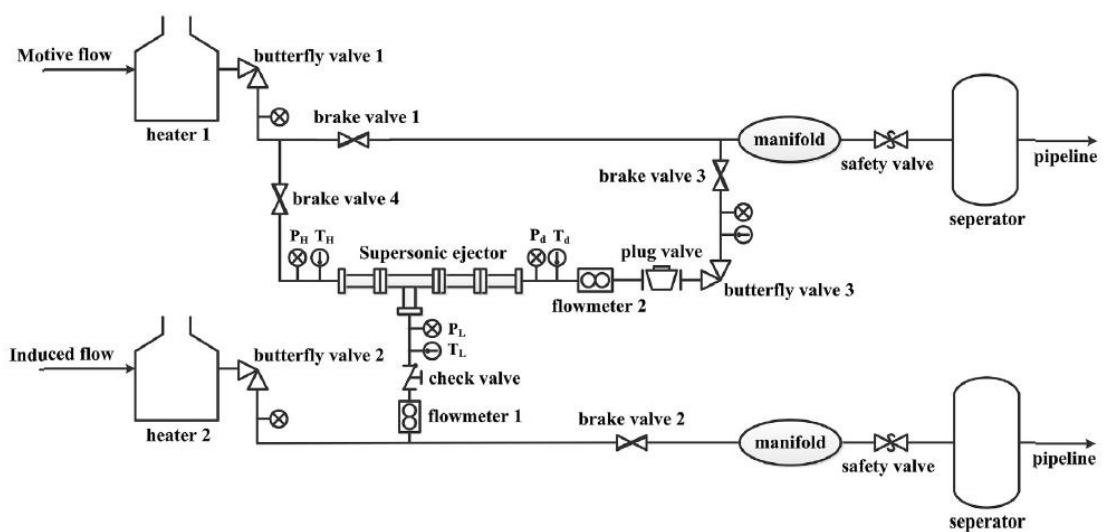


**Figure 2.12 Schematic of test system of supersonic natural gas ejector (TSED)**

Chen et al. (2013: 33 - 40) [32] presented a two-stage ejector mechanical compression performance to improve the COP of the ejector cooling cycle intended for micro-trigeneration. The first stage process was realized by a mechanical compressor, while the second stage by an ejector. The cooling cycle process had Ammonia (R717) as the working fluid, and the evaporator provided temperatures ranging from -10 to 5 °C. Analysis of the two-stage cooling cycle showed that the COP increased and the highest ratio and cooling capacity of 10 kW intended for application in the micro-trigeneration system. Two-stage cooling systems reduced the electrical power consumption by 34.5% compared to electrically-driven of vapor compression cooling systems.

## 2.6 Ejector applications

Jenn-Jiang Hwang (2014: 256 - 263) [33] described the development of a passive hydrogen recovery scheme using a vacuum ejector for the anode of a proton exchange membrane (PEM) fuel cell system. The vacuum ejector connected anode outlet to entrain the unused hydrogen into hydrogen supply. Two different combinations of a continuous-flow mode and a pulse-flow mode in the hydrogen supply were introduced. The results showed the constant system load of 1.45 kW, the entrainment ratio of ejector between 40-50%, and the efficiency of the system which varied between 35-48%. Afterward, Jenn-Jiang Hwang et al. revealed the anode off-gas in a proton exchange membrane fuel cell (PEMFC) system with a higher entrainment ratio [34]. It increased the mass flow rate in the suction channel of the PEMFC system with 3-D numerical simulation.

The system performance of the solar-driven ejector refrigeration technology applications depends on the type of refrigerant, the operating conditions, and the ejector geometry [35]. Using computer simulation and test analysis, three different solar collectors were selected to drive the solar ejector air conditioning system and resulted with the system high-performance heat pipe [36]. The computational fluid dynamics of a solar-driven variable geometry ejector showed that the mixing phenomenon was the major parameter; the ejector performance was improved by 37% [37]. Meanwhile, the TRaNsient System Simulation program (TRNSYS) for analysis of a solar-driven air conditioning system which composed of four main subsystems, including solar loop, ejector cycle, PCM cold storage, and air-conditioned space showed that the cold storage optimal volume of 1,000 liters was the highest cooling COP. The maximum COP and solar thermal ratio (STR) were 0.193 and 0.097, respectively [38].

Besides, the air cooling of turbocharged gasoline engines used the ejector with an exhaust gas driven jet-ejector cooling system to increase engine efficiency [39]. There were also several ejector usage including an ejector of the appropriate condenser vacuum pump system of a steam turbine power plant [40], an ejector replacing mechanical compressors or combining with mechanical compressors in the refrigeration systems [41], and ejector vacuum filters in cake dewatering [42].

Various ejector refrigeration systems were described with the associated studies, and categorized as conventional ejector refrigeration system, combined refrigeration systems, advanced ejector refrigeration systems/Multi-components ejector refrigeration system (MERS) [43, 44]. The MERS geometric structure, such as the two-stage ejector (TSE), greatly affected its performance. The design concept of the proposed two-stage ejector was first invented by Grazzini in 1998 which classified it into two types including annular primary and annular secondary, at the second stage. By the simulation results, it showed that the annular primary generated high ejector compression ratio with a very compact geometrical configuration but low entrainment ratio [45, 46], and annular secondary increased performance in terms entrainment ratio of a conventional single-stage ejector [47-49]. For refrigeration applications, the two most important parameters used to describe the performance of an ejector specified in terms of entrainment ratio ( $R_m$ ) and critical back pressure (CBP).  $R_m$  is the ratio of mass flow rate between the secondary and the primary fluid entering the ejector. The critical back pressure (CBP) implies the condensing pressure in the real system where the flow is choked and remains stable [50]. The typical performance curve between ejector back pressure and the  $R_m$  of a steam ejector is shown in Figure 2.3. There are three operating regions distinguished by the back pressure in the ejector.

This study presents an investigation of the performance of the two-stage ejector (TSE) using computational fluid dynamics (CFD) validation with experimental results and compared with the single-stage ejector (SSE).

## **CHAPTER 3**

### **RESEARCH METHODOLOGY**

The finite volume method used computational fluid dynamics (CFD) to compare performance of two-stage ejector (TSE) and single-stage ejector (SSE) for refrigeration system application and the gas/gas ejector application. Also, the CFD results were validated with experimental results data.

#### **3.1 Computation fluid dynamic (CFD)**

An analysis of CFD simulations used the commercial software FLUENT 6.3. The geometry and mesh generation of an ejector used the software GAMBIT 2.3. This study is to investigate the performance of gas/gas ejector applications by using the CFD approach compared with a single-stage ejector (SSE). Moreover, validation of the CFD results with the real experiments were also performed so that the results could be credible.

##### **3.1.1 CFD Technical data for the current study**

The supersonic flow inside the ejector flow of the refrigeration system depends on the working condition of the model.

###### **3.1.1.1 Turbulence model**

The shear-stress-transportation  $k-\omega$  ( $k-\omega$ -sst) turbulence viscosity model was utilized for simulating the ejector flow which provided more accurate results [5, 51-53]. The mixing flows, shock wave, and shear layers governing equations can be written as follows:

Continuity:

$$\frac{\partial \rho}{\partial t} + \frac{\partial}{\partial x_i} (\rho u_i) = 0 \quad (3.1)$$

Momentum:

$$\frac{D(\rho u_i)}{Dt} = -\frac{\partial p}{\partial x_i} + \frac{\partial}{\partial x_j} \left[ \mu_{eff} \left( \frac{\partial u_i}{\partial x_j} + \frac{\partial u_j}{\partial x_i} - \frac{2}{3} \delta_{ij} \frac{\partial u_k}{\partial x_k} \right) \right] + \frac{\partial}{\partial x_j} \left( -\overline{\rho u_i' u_j'} \right) \quad (3.2)$$

The velocity was given as the mass-averaged values. Turbulent heat transport was modeled using the Reynolds analogy to calculate turbulent momentum transfer.

The modeled energy equation:

$$\frac{\partial}{\partial t} (\rho E) + \frac{\partial}{\partial x_j} [u_j (\rho E + p)] = \frac{\partial}{\partial x_j} \left[ \left( \alpha + \frac{C_p \mu_t}{P_r} \right) \frac{\partial T}{\partial x_j} + \mu_i (\tau_{ij})_{eff} \right] \quad (3.3)$$

Energy and temperature were represented by mass-averaged values. The default value of the turbulent Prandtl number (Prt) is 0.85.

Generally, the flow field in the ejector will reach up to supersonic speed; therefore the compressible axis-symmetric Navier-Stokes equations are suitable for the analysis of variable density flows. In this simulation and prediction of the performance, the density-based implicit solver was selected to solve the governing equations. The turbulence model was applied to the whole flow domain based on the shear-stress-transportation k- $\omega$  turbulence. The turbulence kinetic energy (k) and specific dissipation rate ( $\omega$ ) can be obtained from these equations:

$$\frac{\partial}{\partial t} (\rho k) + \frac{\partial}{\partial x_i} (\rho k u_i) = \frac{\partial}{\partial x_j} \left( \Gamma_k \frac{\partial k}{\partial x_j} \right) + G_k - Y_k + S_k \quad (3.4)$$

$$\frac{\partial}{\partial t} (\rho \omega) + \frac{\partial}{\partial x_j} (\rho \omega u_j) = \frac{\partial}{\partial x_j} \left( \Gamma_\omega \frac{\partial \omega}{\partial x_j} \right) + G_\omega - Y_\omega + D_\omega + S_\omega \quad (3.5)$$

where  $\Gamma_k$  and  $\Gamma_\omega$  represent the effective diffusivity of k and  $\omega$ ,  $G_k$  and  $G_\omega$  represent the production of turbulence kinetic energy and the generation of  $\omega$ ,  $Y_k$  and  $Y_\omega$  represent the dissipation of k and  $\omega$ ,  $S_k$  and  $S_\omega$  are user-defined source terms, and  $D_\omega$  is the cross-diffusion term.

### 3.2 Refrigeration system application

#### 3.2.1 The single-stage ejector

For geometric structure of a single-stage ejector in the steam ejector refrigeration, the dimensions were designed by Ruangtrakoon and Aphornratana (2014: 142 - 152) [54]. The major parameters of the calculated domains are shown in Figure 3.1 and Table 3.1.

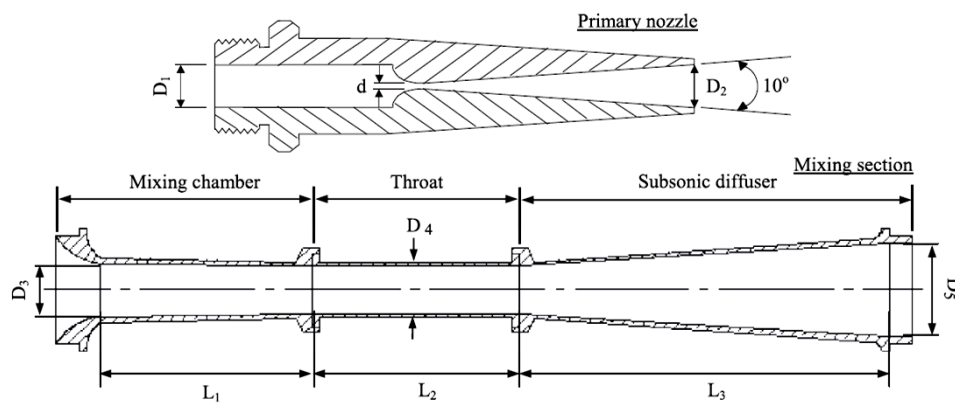


Figure 3.1 The single-stage ejector used in the research study [54]

Table 3.1 Parameters of the single-stage ejector [54]

Parameter	Value (mm)
Diameter of nozzle (d)	3.8
Diameter of entrance nozzle (D <sub>1</sub> )	13.0
Nozzle area ratio [(D <sub>2</sub> /d) <sup>2</sup> ]	20.0
Diameter of entrance mixing chamber (D <sub>3</sub> )	34.0
Diameter of throat (D <sub>4</sub> )	33.0
Diameter of exit subsonic diffuser (D <sub>5</sub> )	60.0
Distance of mixing chamber (L <sub>1</sub> )	135.0
Distance of throat (L <sub>2</sub> )	138.0
Distance of subsonic diffuser (L <sub>3</sub> )	242.0

The commercial software Gambit 2.3 and FLUENT 6.3 were used for the grid generation and the CFD solver, respectively. Two-dimensional (2-D) axisymmetric model was used as suggested by Pianthong et al. (2007: 2556-2564) [55]. The shear-stress-transportation  $k-\omega$  ( $k-\omega$ -sst) turbulence viscosity model which provided significantly accurate results [50, 53] was used. The properties of water vapour are shown in Table. 3.2, the density of the working fluid was evaluated by using the ideal gas relationship during the progress of the calculation.

**Table 3.2 Properties working fluid (water vapour) used in the CFD simulation**

Properties	Value
Viscosity, $\mu$ (kg/m s)	$1.34 \times 10^{-5}$
Thermal conductivity, $k$ (W/m k)	0.0261
Specific heat capacity, $C_p$ (J/kg K)	2014.00
Molecular weight, $M$ (kg/kmol)	18.01534

All dimensions of the calculation domain shown in Figure 3.2, the grids were made of 55,000 structured quadrilateral elements. The ejector investigation of the effects of geometry on the flow of the steam ejector was performed, as well as a grid refinement which increased the grid numbers to around 80,000. After refining the grid elements, the solutions of the models with the order of 40,000 elements and 80,000 elements found no difference [54]. The entrainment ratio ( $R_m$ ) of the single-stage ejector is defined by the following equation:

$$R_{m_{\text{single-stage}}} = \frac{\dot{m}_s}{\dot{m}_p} \quad (3.1)$$

where  $\dot{m}_p$  is the mass flow rate of the primary fluid and  $\dot{m}_s$  is the mass flow rate of secondary fluid

### 3.2.2 The two-stage ejector

The flow phenomena in ejectors is more complicated than that of the SSE. In an SSE, a high-pressure steam known as “a primary fluid” expands and accelerates through the primary nozzle, it fans out with supersonic speed to create a very low-pressure region at the nozzle exit plane subsequently in the mixing chamber. The fluid of low-pressure “a secondary fluid” then can flow into the mixing chamber. This mixing causes the primary flow to be retarded while the secondary flow is accelerated. By the end of the ejector, the two streams are completely mixed.

The design concept of the proposed two-stage ejector is an annular secondary at the second stage compared with the single-stage ejector. All dimensions are similar to those of the SSE unless the distance of the throat ( $L_2$ ). The length of  $L_2$  decreases according to the length of  $L_4$  which is called  $L_2'$ , where the total length ( $L_4+L_2'$ ) is 138 mm.

This study is to investigate the performance of the two-stage ejector, which is annular secondary, the effects of the mixing chamber geometries at the second-stage in three-effect parameter systems,  $A_6$ ,  $L_4$ , and  $\theta_{II}$ . The dimensions of the geometry domain are shown in Figure 3.3. The grids were made up of 70,000 structured quadrilateral elements. The grid independence was tested to guarantee the reliability and accuracy of the simulation.

The entrainment ratio for two-stage ejector (TSE) is the ratio between the sum of the secondary fluid mass flow rate (at the first stage and the second stage) and the primary fluid mass flow rate which can be written as

$$Rm_{\text{two-stage}} = \frac{\dot{m}_{s,1} + \dot{m}_{s,2}}{\dot{m}_p} \quad (3.2)$$

where  $\dot{m}_p$  is the mass flow rate of the primary fluid,  $\dot{m}_{s,1}$  is the mass flow rate of secondary fluid at the first stage and  $\dot{m}_{s,2}$  is the mass flow rate of secondary fluid at the second stage

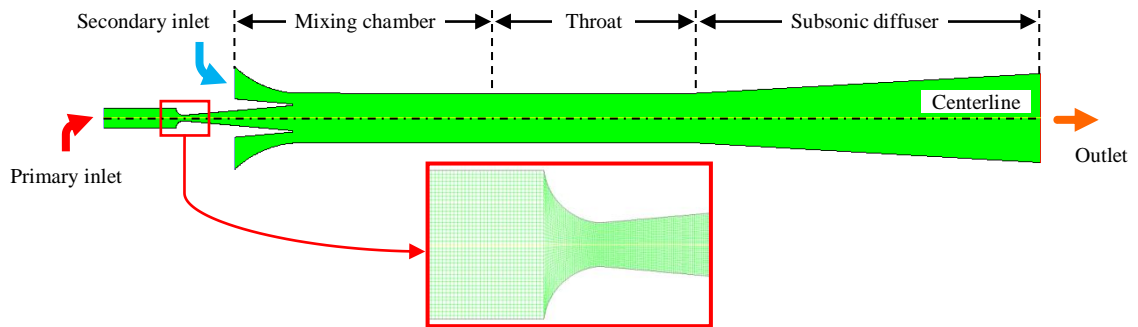


**Figure 3.2 Geometry domain and grid structure of the single-stage ejector CFD model [54]**

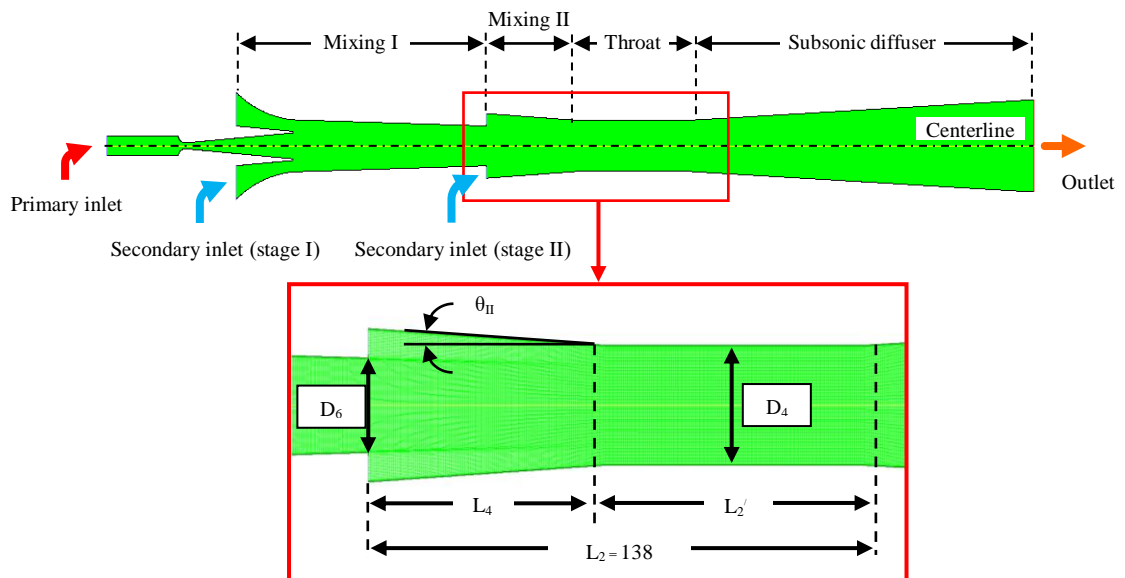


**Figure 3.3 Geometry domain and grid structure of the two-stage ejector type annular secondary at second stage CFD model**

### 3.3 The gas/gas ejector application

#### 3.3.1 Ejector nozzle design

The flow rate of the primary inlet calculated using the theory of compressible gas flow through a convergent-divergent nozzle which is the maximum mass flow rate for a given throat diameter defined by the following equation:

$$\dot{m}_p = \frac{A_t P_p}{\sqrt{\frac{RT_p}{k} \left(\frac{k+1}{2}\right)^{\left(\frac{k+1}{k-1}\right)}}} \quad (3.3)$$

Thus, the cross-sectional area at the throat of the primary nozzle can be written as:

$$A_t = \frac{\dot{m}_p}{P_p} \sqrt{\frac{RT_p}{k} \left(\frac{k+1}{2}\right)^{\left(\frac{k+1}{k-1}\right)}} \quad (3.4)$$

Applying the continuity equation of an ideal gas, the cross-sectional area at the primary nozzle exit can be written as:

$$\frac{A_{1'}}{A_t} = \frac{\left(\frac{2}{k+1}\right)^{\left(\frac{1}{k-1}\right)} \times \sqrt{1 - \left(\frac{2}{k+1}\right)}}{\left(\frac{P_1}{P_p}\right)^{\left(\frac{1}{k}\right)} \times \sqrt{1 - \left(\frac{P_1}{P_p}\right)^{\left(\frac{k-1}{k}\right)}}} \quad (3.5)$$

Where the cross-sectional area of the secondary fluid at the inlet of the mixing chamber can be written as:

$$\frac{A_{1''}}{A_t} = \frac{Rm \sqrt{\frac{T_s}{T_p} \left(\frac{2}{k+1}\right)^{\left(\frac{1}{k+1}\right)} \left(\frac{P_p}{P_s}\right) \left(\frac{P_s}{P_1}\right)^{\left(\frac{1}{k}\right)}}}{\sqrt{\frac{k+1}{k-1} \left[1 - \left(\frac{P_1}{P_s}\right)^{\left(\frac{k-1}{k}\right)}\right]}} \quad (3.6)$$

The mixing chamber inlet diameter when a zero thickness of the primary nozzle exit's wall assumed, can be written as:

$$A_1 = A_{1'} + A_{1''} \quad (3.7)$$

### 3.3.2 Computational fluid dynamics (CFD) model

Gambit 2.3 and FLUENT 6.3 were used for the grid generation and the CFD solver, respectively. Two-dimensional (2-D) axisymmetric model and the shear-stress-transportation  $k-\omega$  ( $k-\omega$ -sst) turbulence viscosity model was used. The properties of air are shown in Table 3.3, the density of the working fluid was evaluated by using the ideal gas relationship during the progress of the calculation.

The design of the single-stage ejector and the two-stage ejector used response surface methodology (RSM). The RSM is a collection of mathematical and statistical techniques for empirical model building. The methodology can be used to find the relationship between random input variables and output response through probabilistic analysis and regression analysis. The application of RSM was optimized to design the SSE and TSE geometry significant factors which were 8 and 10, respectively, and investigations were analyzed using the RSM on 282 runs and 542 runs, respectively. The result of RSM analyzes optimum solutions for the SSE and the TSE are presented in Table 3.4 and Table 3.5, respectively. The grids of SSE and TSE structured quadrilateral elements were made of 89,200 and 102,800, respectively.

**Table 3.3 Properties working fluid (air) used in the CFD simulation**

Properties	Value
Viscosity, $\mu$ (kg/m s)	$1.7894 \times 10^{-5}$
Thermal conductivity, $k$ (W/m k)	0.0242
Specific heat capacity, $C_p$ (J/kg K)	1006.43
Molecular weight, $M$ (kg/kmol)	28.966

**Table 3.4 The RSM analyzed optimum solutions the SSE**

Factor	Name	Units	Minimum	Maximum	optimum solutions
A	Primary inlet pressure	bar	4	7	4
B	Secondary inlet pressure	bar	0.5	1	1
C	Area ratio of $A_3/A_6$		2	2.5	2.5
D	Area ratio of $A_6/A_1$		5	10	10
E	Area ratio of $A_7/A_6$		2	5	5
F	Convergence angle of mixing chamber	deg.	2	10	10
G	Length ratio of $L_2/D_6$		1	3	1
H	Convergence angle of subsonic diffuser	deg.	3	7	3

**Table 3.5 The RSM analyzed optimum solutions the TSE**

Factor	Name	Units	Minimum	Maximum	optimum solutions
A	Primary inlet pressure	bar	4	7	4
B	Secondary inlet pressure	bar	0.5	1	1
C	Area ratio of $A_3/A_4$		2	2.5	2.5
D	Area ratio of $A_4/A_6$		0.5	1	0.5
E	Convergence angle of mixing chamber II	deg.	2	10	10
F	Area ratio of $A_6/A_1$		5	10	10
G	Area ratio of $A_7/A_6$		2	5	5
H	Convergence angle of mixing chamber I	deg.	2	10	10
J	Length ratio of $L_2/D_6$		1	3	3
K	Convergence angle of subsonic diffuser	deg.	3	7	7

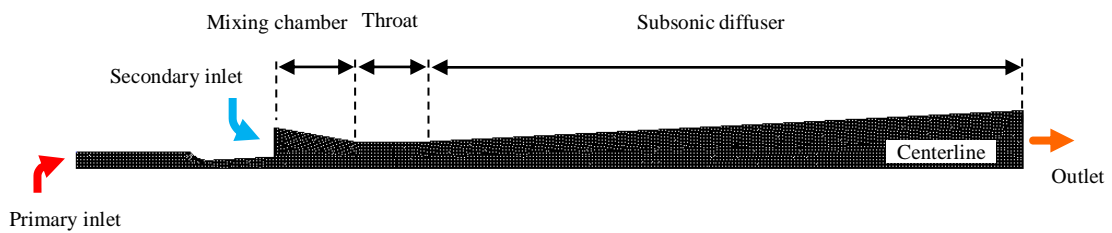


**Figure 3.4 Geometry domain and grid structure of the SSE gas/gas ejector CFD model**

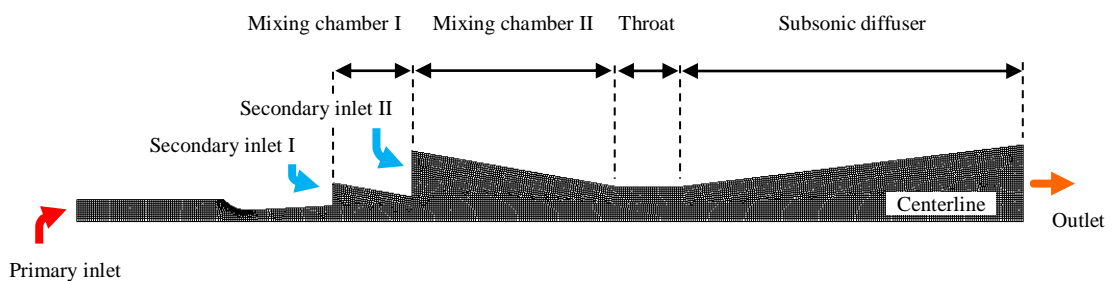


**Figure 3.5 Geometry domain and grid structure of the TSE gas/gas ejector type annular secondary at second stage CFD model**

### 3.3.2 Experimental apparatus

The system scheme and the experimental configuration of SSE built in the gas/gas ejector application are shown in Figure 3.6 and Figure 3.7, respectively. While those of the TSE are shown in Figure 3.8 and Figure 3.9, respectively. Experimental SSE and TSE are the proposal of a double-evaporator ejector refrigeration system. The system has 5 major components: a vapor-generator, a two-stage ejector, a condenser, a evaporator, and a pump. The steam ejector refrigeration system was investigated by using the operating conditions from the previous work, an operating pressure of primary inlet (4-5 bar), secondary inlet (0.8-0.9 bar) were specified.

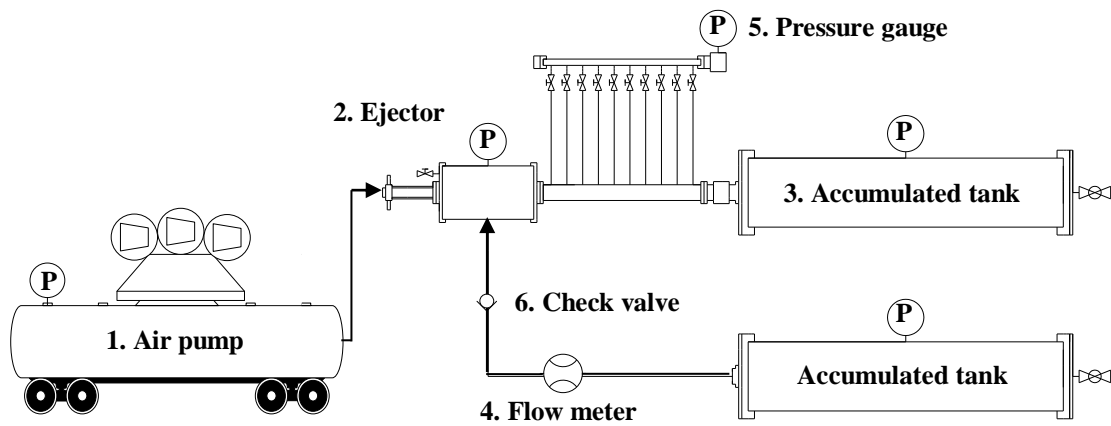


**Figure 3.6 System scheme of the SSE in the gas/gas ejector system**



**Figure 3.7 The experimental SSE gas/gas ejector system**

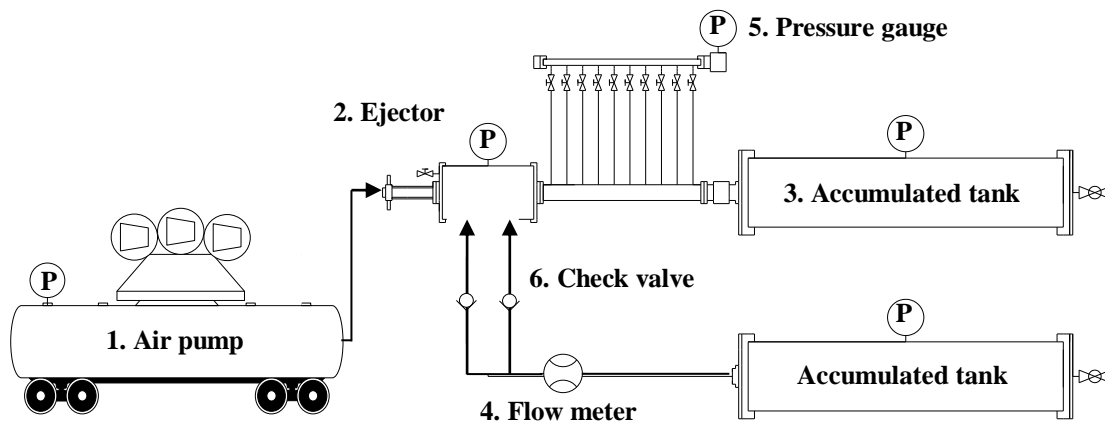


**Figure 3.8 System scheme of TSE in the gas/gas ejector**



**Figure 3.9 The experimental TSE gas/gas ejector system**

### 3.3.2.1 Primary nozzle

The schematic dimensional and photograph of the primary nozzle in the gas/gas ejector system installed in the experiment rig, as shown in Figure 3.10 and Figure 3.11, respectively.

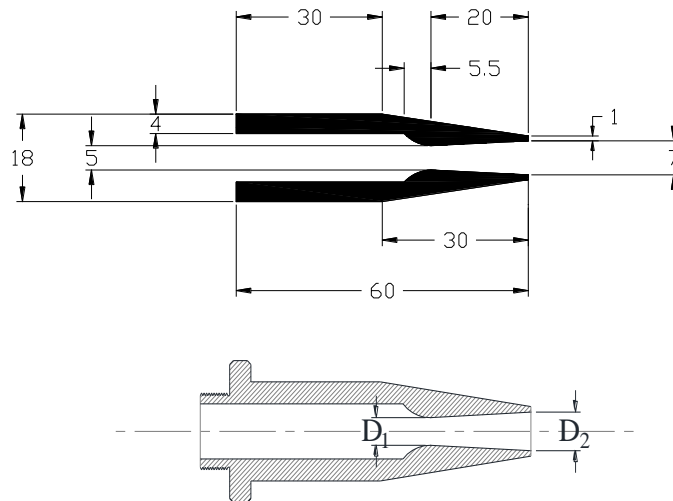


**Figure 3.10 Dimensional of the primary nozzle in the gas/gas ejector system  
(scale : mm)**



**Figure 3.11 Photograph of the primary nozzle in the gas/gas ejector system**

### 3.3.2.2 The single-stage ejector

The schematic dimensional and photograph of the single-stage ejector in the gas/gas ejector system installed in the experiment rig, as shown in Figure 3.12 and Table 3.6, respectively.

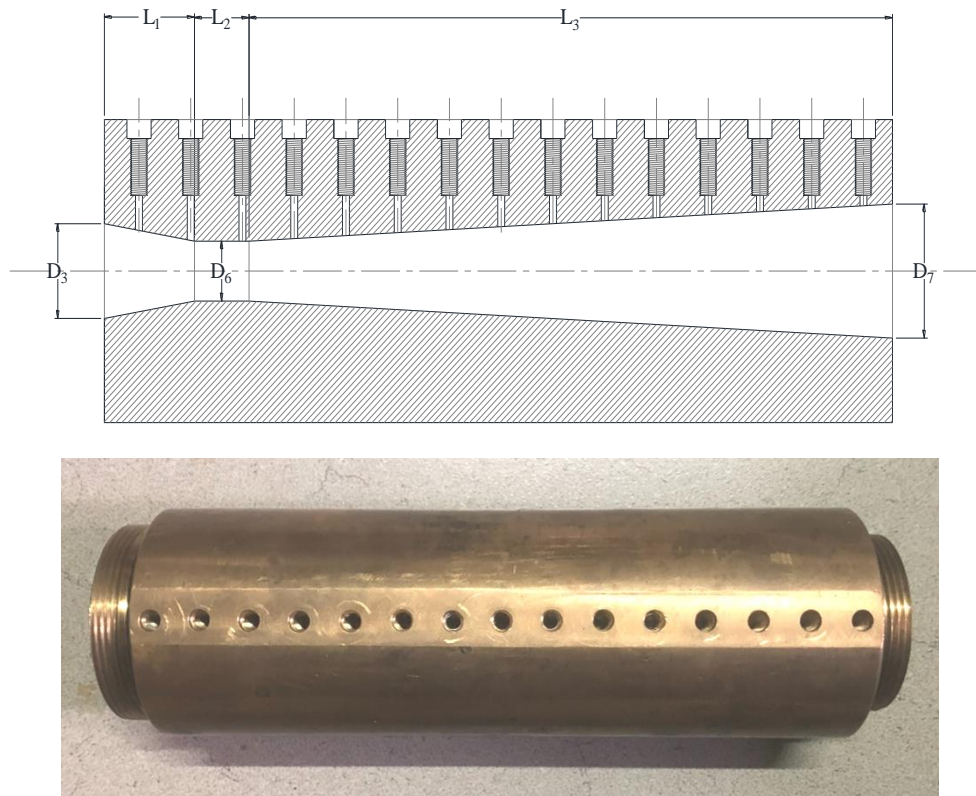


**Figure 3.12 Photograph of the single-stage ejector in the gas/gas ejector system**

**Table 3.6 Parameters of the single-stage ejector in the gas/gas ejector system**

Parameter	Value (mm)
Diameter of entrance mixing chamber ( $D_3$ )	25.0
Diameter of throat ( $D_6$ )	15.8
Diameter of exit subsonic diffuser ( $D_7$ )	35.4
Distance of mixing chamber ( $L_1$ )	26.1
Distance of throat ( $L_2$ )	15.8
Distance of subsonic diffuser ( $L_3$ )	186.5

### 3.3.2.3 The two-stage ejector

The schematic dimension and photograph of the two-stage ejector in the gas/gas ejector system were installed in the experiment rig, as shown in Figure 3.13 and Table 3.7, respectively.

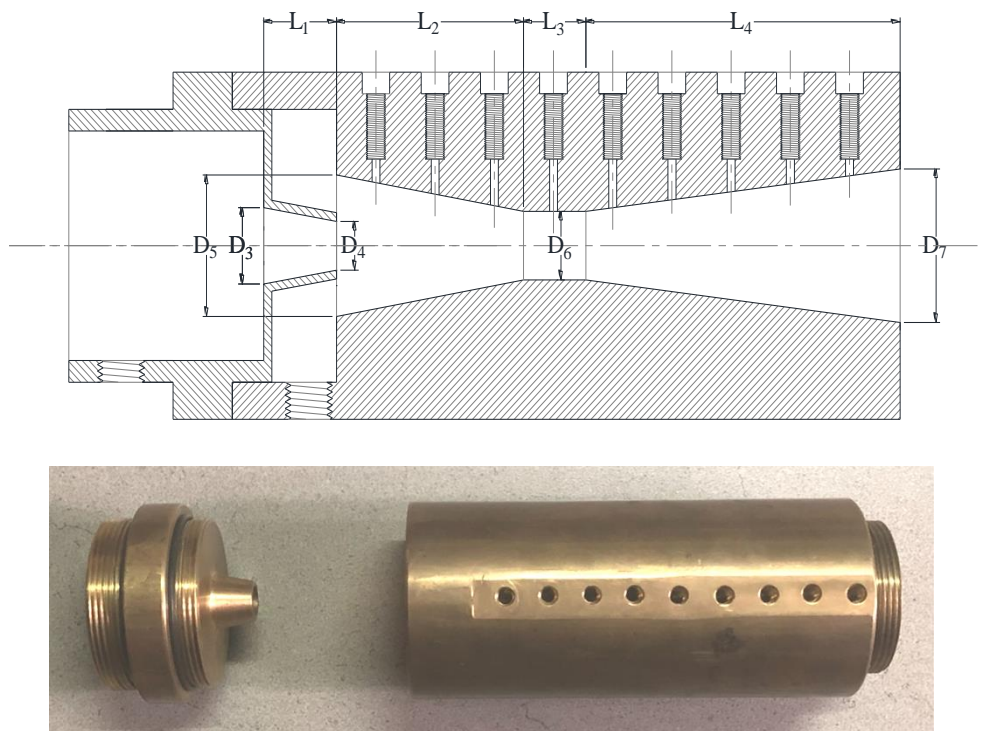


**Figure 3.13** Photograph of the two-stage ejector in the gas/gas ejector system

**Table 3.7** Parameters of the two-stage ejector in the gas/gas ejector system

Parameter	Value (mm)
Diameter of entrance mixing chamber ( $D_3$ ) at the first stage	17.6
Diameter of exit mixing chamber ( $D_4$ ) at the first stage	11.2
Diameter of entrance mixing chamber ( $D_5$ ) at the second stage	32.6
Diameter of throat ( $D_6$ )	15.8
Diameter of exit subsonic diffuser ( $D_7$ )	35.4
Distance of mixing chamber ( $L_1$ ) at the first stage	18.4
Distance of mixing chamber ( $L_2$ ) at the second stage	47.4
Distance of throat ( $L_3$ )	15.8
Distance of subsonic diffuser ( $L_4$ )	79.6

### 3.3.2.4 The pumping system

The primary inlet pressure of the gas/gas ejector system was generated by PUMA type PP-315 (15 HP), which are capacity at the pressure of 2,850 l/min at 8 kg/cm<sup>2</sup>, air tank capacity of 315 liters, and working pressure of 8-10 kg/cm<sup>2</sup>.

### 3.3.2.5 The instruments

The instruments ranges and accuracies of the gas/gas ejector system are presented in Table 3.8

**Table 3.8 Instruments introduction**

<b>Instruments</b>	<b>Range</b>	<b>Accuracy</b>
Pressure gage NUOVA FIMA	0 to 2.5 bar 0 to 6 bar -1 to 1.5 bar -1 to 5 bar	1,6 as per EN 837-1.
Float flow meter NITTO VA10S-40	12 to 120 m <sup>3</sup> /h	± 2.5% (Full scale)

## CHAPTER 4

### RESULTS AND DISCUSSIONS

This chapter provides the investigation results of the ejector refrigeration system and gas/gas ejector system. The results from different operating conditions on the performance characteristics were evaluated in terms of the entrainment ratio ( $R_m$ ) and the critical back pressure (CBP).

#### 4.1 CFD results of ejector refrigeration system

In the simulation, the TSE refrigeration system was investigated by using the operating conditions from the previous work [54] with generator temperature ( $T_g$ ) of 110 °C and the evaporator temperature ( $T_e$ ) of 10 °C. The performance of the single-stage ejector at the maximum cooling load of 3000 W and the room temperature of 24.2 °C were obtained. The entrainment ratio of the single-stage ejector was 0.50, and the COP was raised to the maximum value at 0.45 [54].

The effects of the area ratio ( $A_4/A_6$ ) in the mixing chamber geometries at the second stage on the entrainment ratio shows in “Figure 4.1”. The present numerical study is carried out to investigate the mixing chamber geometries at the second-stage model, with a length ( $L_4$ ) is  $1.0D_4$ , and convergence angle ( $\theta_{II}$ ) is 10°. The TSE system performance provides higher entrainment is 0.665, at the area ratio ( $A_4/A_6$ ) is 1.6 and 1.7.

The effect of the length ( $L_4$ ) in the mixing chamber geometries at the second stage on the entrainment ratio is shown in Figure 4.2. The area ratio of mixing chamber geometries at the second stage ( $A_4/A_6$ ) was 1.6 and convergence angle ( $\theta_{II}$ ) at the second stage was 10°. The maximum entrainment ratio ( $R_m$ ) was 0.694, while the length of the mixing chamber geometries was  $1.6 < L_4/D_4 < 2.0$ .

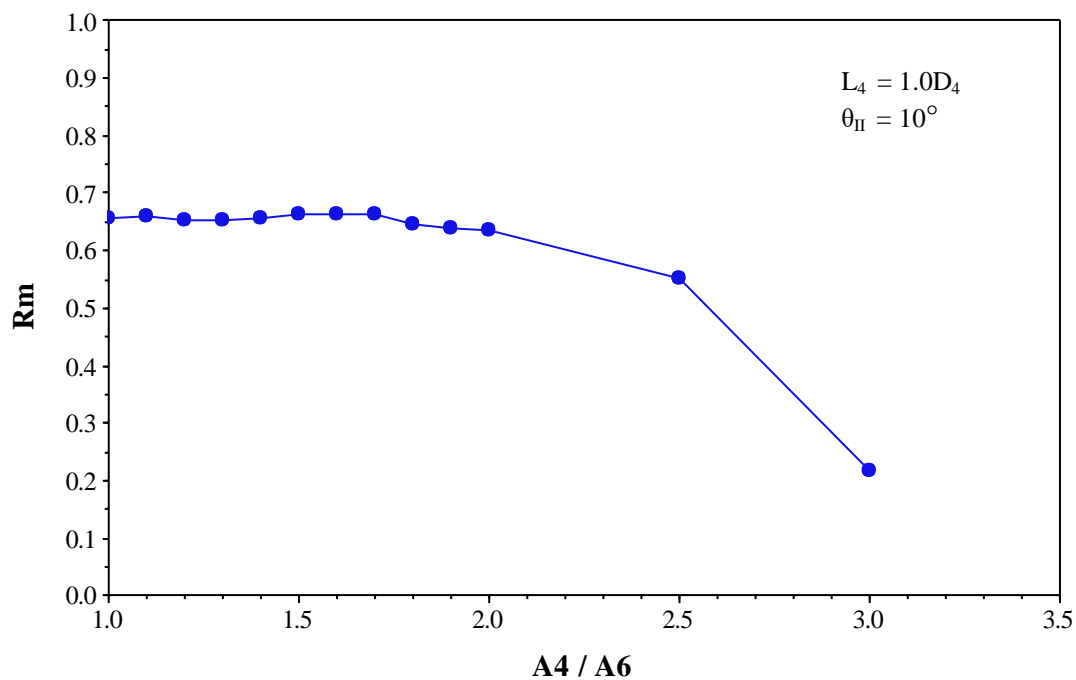


**Figure 4.1** Effect of the area ratio ( $A_4 / A_6$ ) in the mixing chamber geometries at the second stage on the entrainment ratio

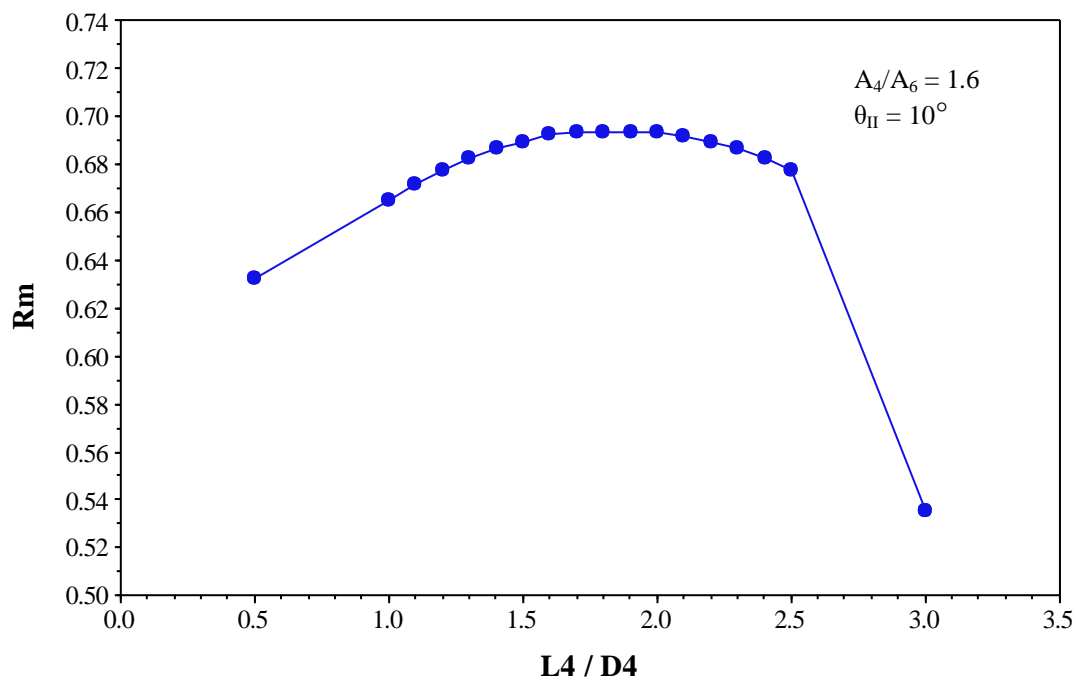


**Figure 4.2** Effect of length ( $L_4$ ) in the mixing chamber geometries at the second stage on the entrainment ratio

The effect of convergence angle ( $\theta_{II}$ ) in the mixing chamber geometries at the second stage on the entrainment ratio is shown in Figure 4.3. The area ratio of mixing chamber geometries at the second stage ( $A_4/A_6$ ) was 1.6 and length ( $L_4$ ) of the mixing chamber at the second stage was  $2.0D_4$ . From the simulations, the TSE provided the maximum entrainment ratio up to 0.714 at convergence angle ( $\theta_{II}$ ) in the mixing chamber of  $4^\circ$ .

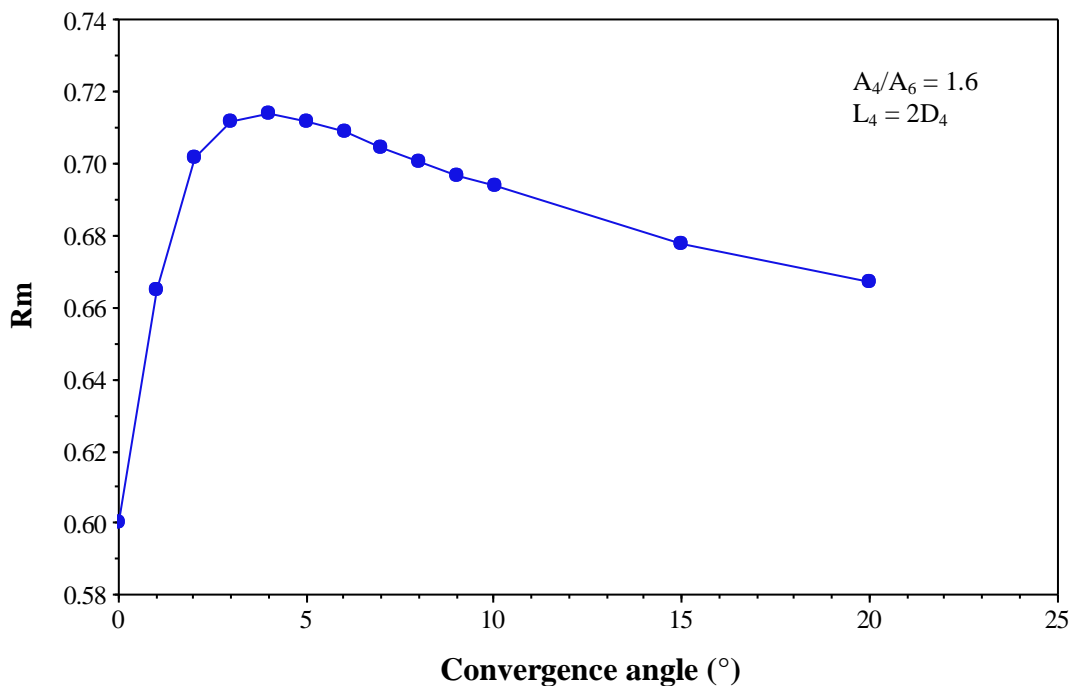


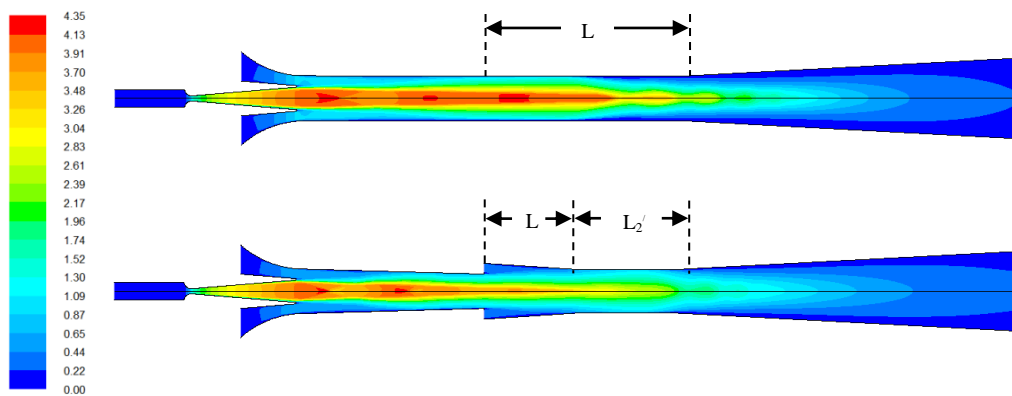
**Figure 4.3 Effect of convergence angle ( $\theta_{II}$ ) in the mixing chamber at the second stage on the entrainment ratio**

The simulation results on an investigation on performance of steam ejector refrigeration system using two-stage ejector type annular secondary at the second stage showed the maximum of entrainment ratio ( $R_m$ ) of 0.714, at the area ratio ( $A_4/A_6$ ) of 1.6, the length ( $L_4$ ) of  $2.0D_4$  and convergence angle ( $\theta_{II}$ ) of  $4^\circ$ . Compared with the single-stage ejector, it increased by 42.8%.

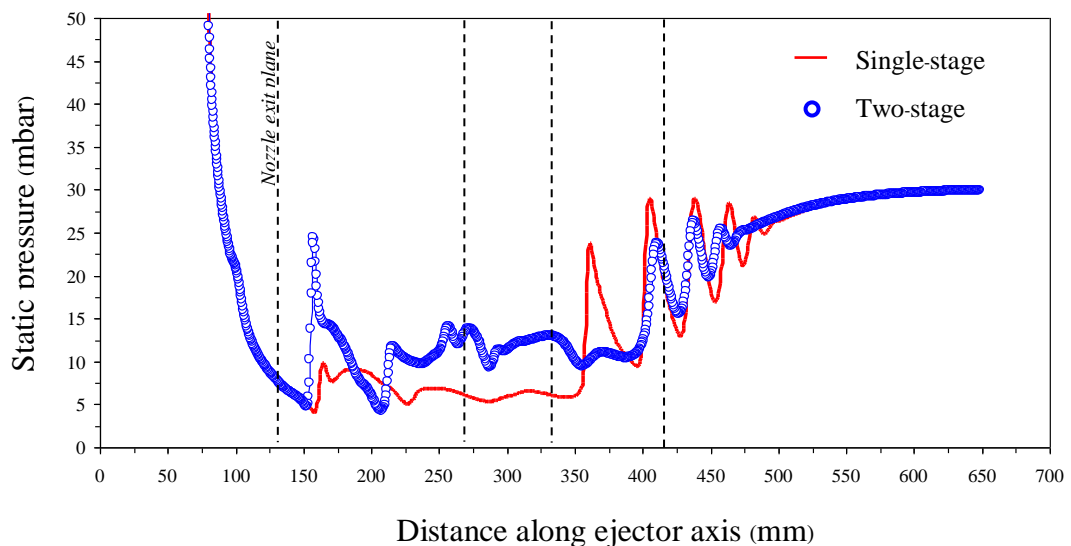
Figure 4.4(a) shows the contours of Mach number of the ejector comparing between single-stage ejector and two-stage ejector. The generator temperature, evaporator, and condenser were fixed at the corresponding saturated temperature of  $110^\circ\text{C}$ ,  $10^\circ\text{C}$ , and  $24.1^\circ\text{C}$  (30 mbar), respectively. The single-stage ejector with a

larger jet core mixing chamber inlet diameter moves with a slightly greater speed and hence a higher momentum. In a two-stage ejector, better mixing of the secondary fluid causes the smaller one.

Figure 4.4(b) shows the static pressure profiles along with the axis of both ejectors. The two-stage ejector has a lower static pressure in the throat ( $L_2'$ ) allowing more secondary flow to be induced. However, in the diverging section, the recovery of the static pressure of the single-stage ejector is better resulting in higher critical back pressure.



(a) Filled contours of Mach number



(b) Static pressure distribution along the centerline of the ejector

**Figure 4.4 Comparison advantages of two-stage ejector and single-stage ejector**

Comparison of CFD results between the secondary mass flow rate of SSE and TSE were under these operating conditions: the area ratio ( $A_4/A_6$ ) of 1.6, the length ( $L_4$ ) of  $2.0D_4$ , the convergence angle ( $\theta_{II}$ ) of  $4^\circ$ , the generator temperature between  $100^\circ\text{C}$  and  $130^\circ\text{C}$ , and the evaporator temperature at  $0, 5, 10,$  and  $15^\circ\text{C}$  which are displayed in Figure 4.5, Figure 4.6, Figure 4.7, and Figure 4.8, respectively. As a results, SSE had better induction of the secondary mass flow rate compared to TSE for both mixing chamber at the first stage ( $\dot{m}_{s,1}$ ) and mixing chamber at the second stage ( $\dot{m}_{s,2}$ ). Moreover, in the mixing chamber of TSE, the second mass flow rate at the first stage was more than that at the second stage. However, decreasing evaporator temperature and increasing generator temperature caused the secondary mass flow rate at the second stage to be more than that at the first stage instead, as described in Figure 4.5.

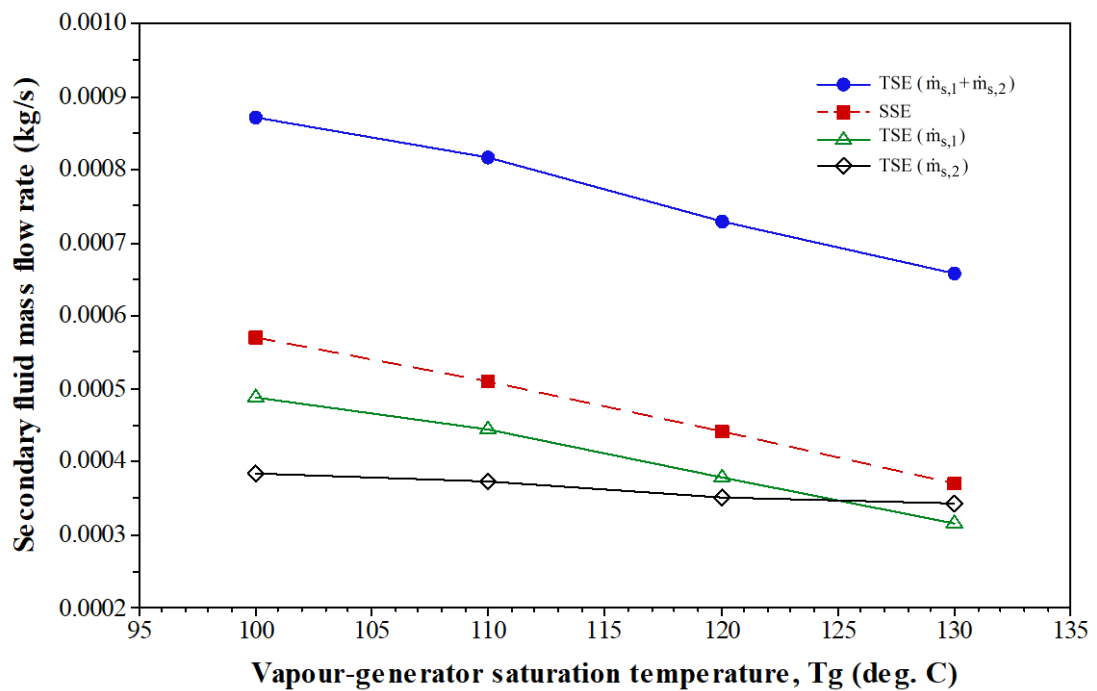


**Figure 4.5 Fluid mass flow rate of SSE and TSE steam ejector at the evaporator temperature of  $0^\circ\text{C}$**

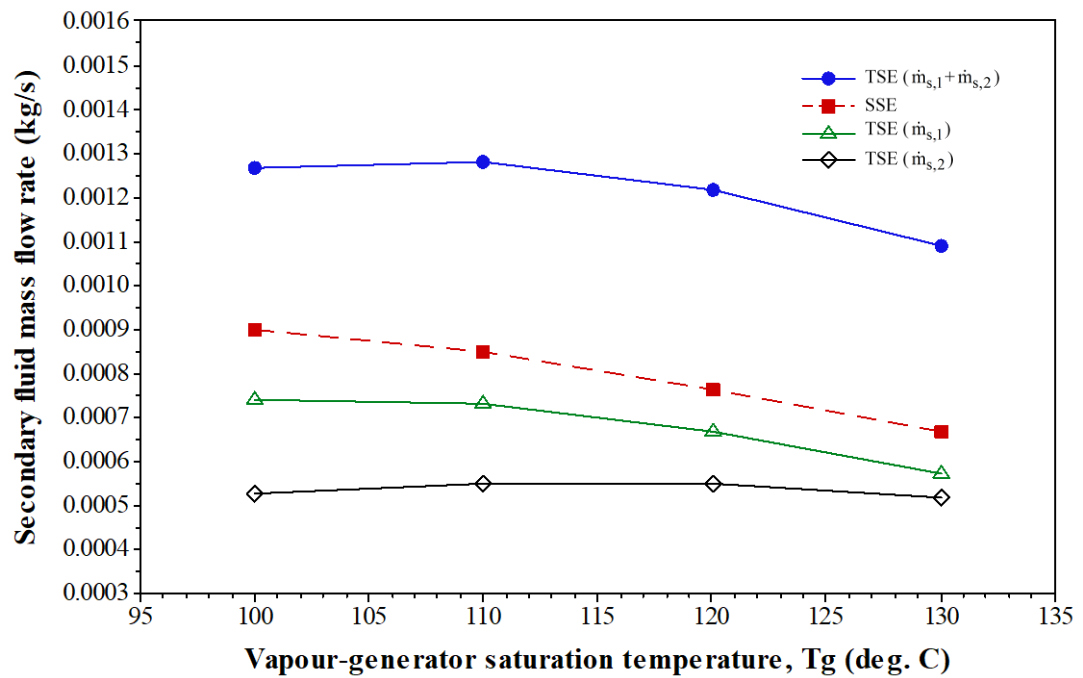


**Figure 4.6 Fluid mass flow rate of the SSE and TSE steam ejector at the evaporator temperature of 5 °C**

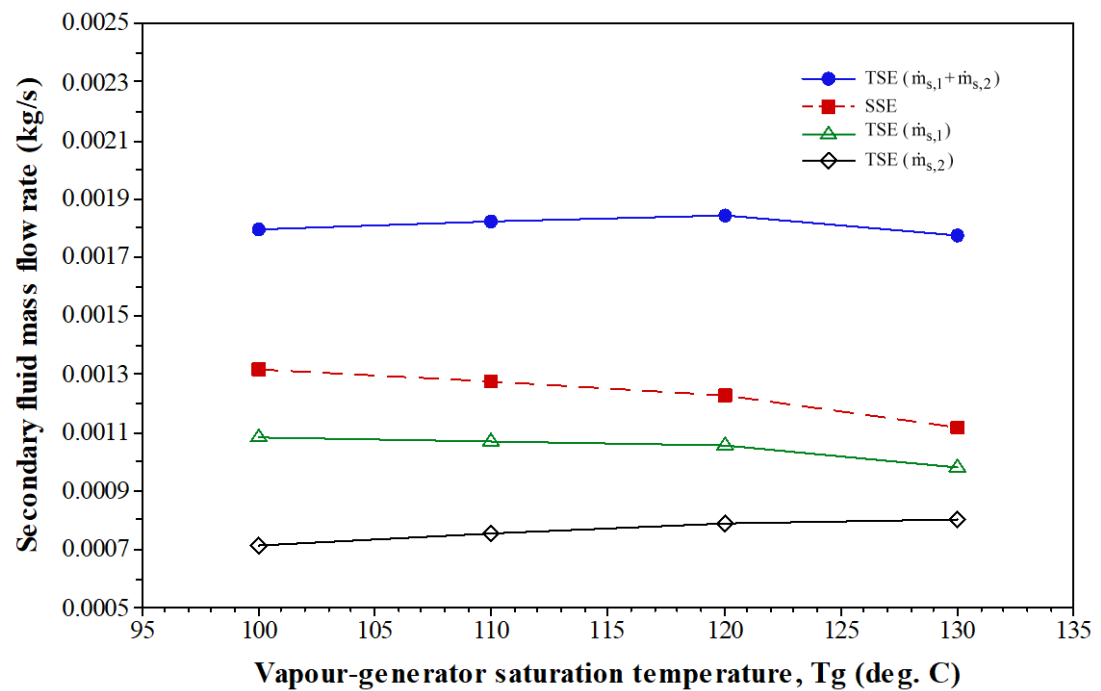


**Figure 4.7 Fluid mass flow rate of the SSE and TSE steam ejector at the evaporator temperature of 10 °C**

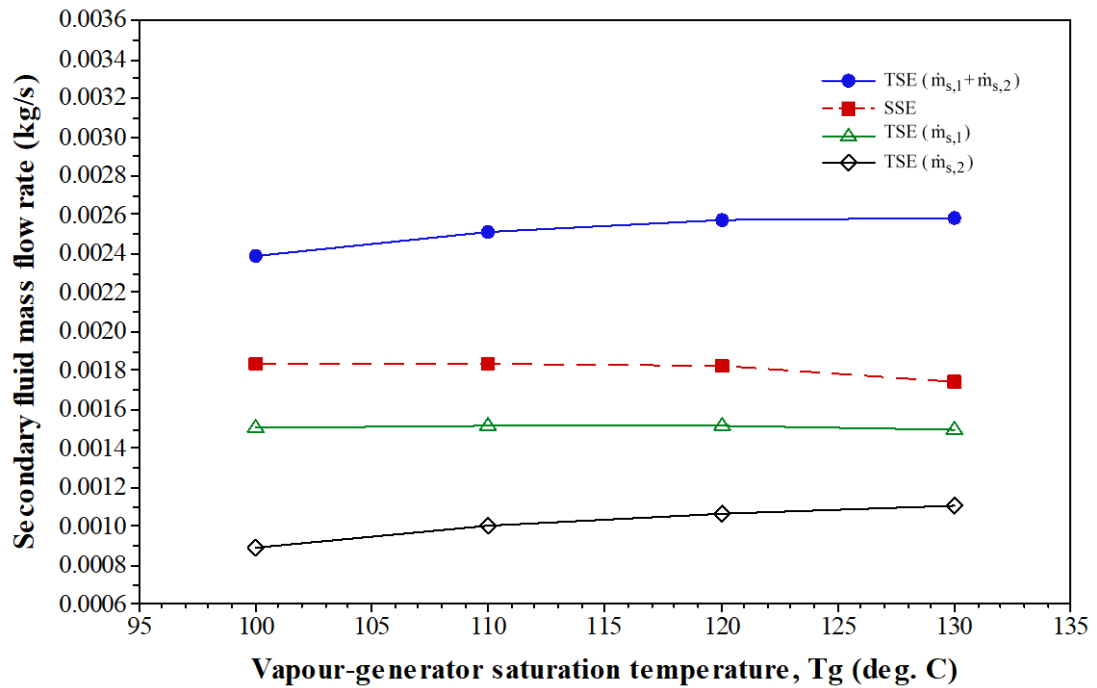


**Figure 4.8 Fluid mass flow rate of the SSE and TSE steam ejector at the evaporator temperature of 15 °C**

Figure 4.9 compares the performance between SSE and TSE, the maximum Rm were equal to 1.000 and 1.307, and the maximum CBP were equal to 60.800 and 55.650 mbar, respectively. At the same working conditions, TSE gained higher Rm but lower CBP compared to SSE. Obviously, under high generator temperature, Rm of both SSE and TSE would reduce but CBP would increase, and for higher evaporator temperature, Rm and CBP of ejector would be higher as well.

The performance of the refrigeration system could be indicated in terms of the Coefficient of Performance (COP), as shown in the equation (4.1).

$$\text{COP} = \text{Rm} \frac{(h_{g,\text{evaporator}} - h_{f,\text{condenser}})}{(h_{g,\text{generator}} - h_{f,\text{condenser}})} \quad (4.1)$$

Coefficient of Performance (COP) of the refrigeration system for SSE and TSE are compared in Figure 4.10. The maximum COP was 0.943 and 1.232, the maximum critical condenser pressure was 60.800 mbar (37.0 deg. C) and 55.650 mbar (34.8 deg. C) for SSE and TSE, respectively. For identical working conditions, TSE could

produce higher COP but lower critical condenser pressure than those of SSE. Furthermore, under high generator temperature, COP of both SSE and TSE will decrease but critical condenser pressure will rise. For higher evaporator temperature, COP and critical condenser pressure of the ejector would also be higher.

Figure 4.11 demonstrates the difference percentage of COP and critical condenser pressure ( $P_{c,cri}$ ) between TSE and SSE, including those of changing the temperature of generator and evaporator. Increasing generator temperature caused the difference percentage of COP for TSE to be higher than that of SSE by 77.2% maximum, but the critical condenser pressure was decreased by 21.9% maximum.

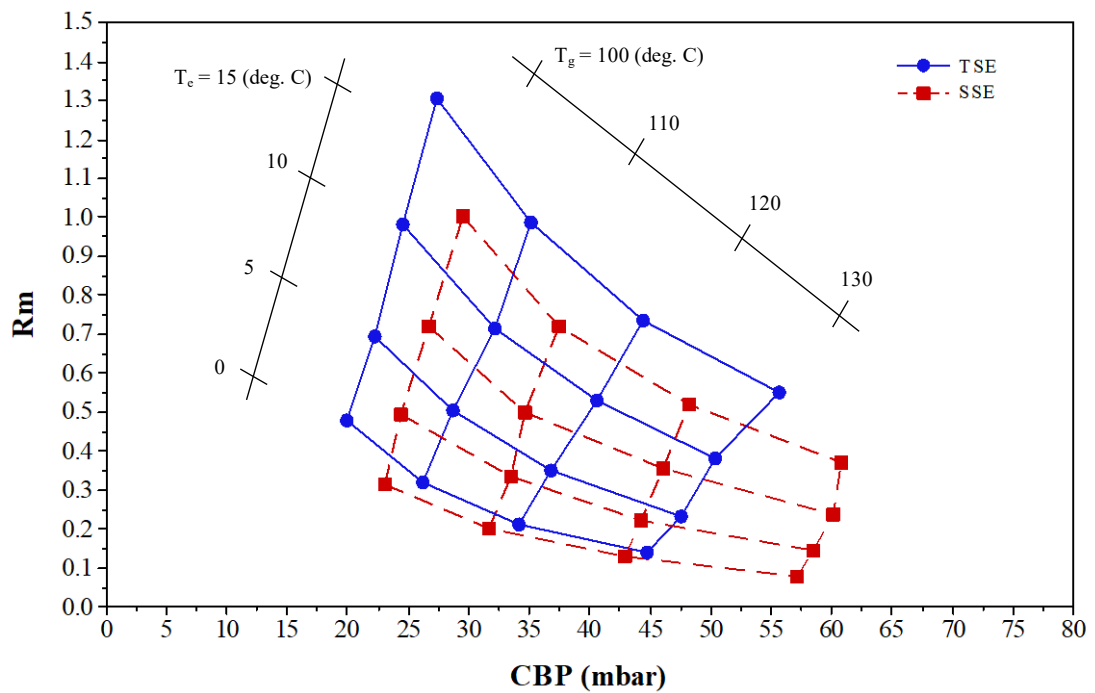


**Figure 4.9 Performance characteristics of the steam ejector, effect of primary and secondary inlet temperature**

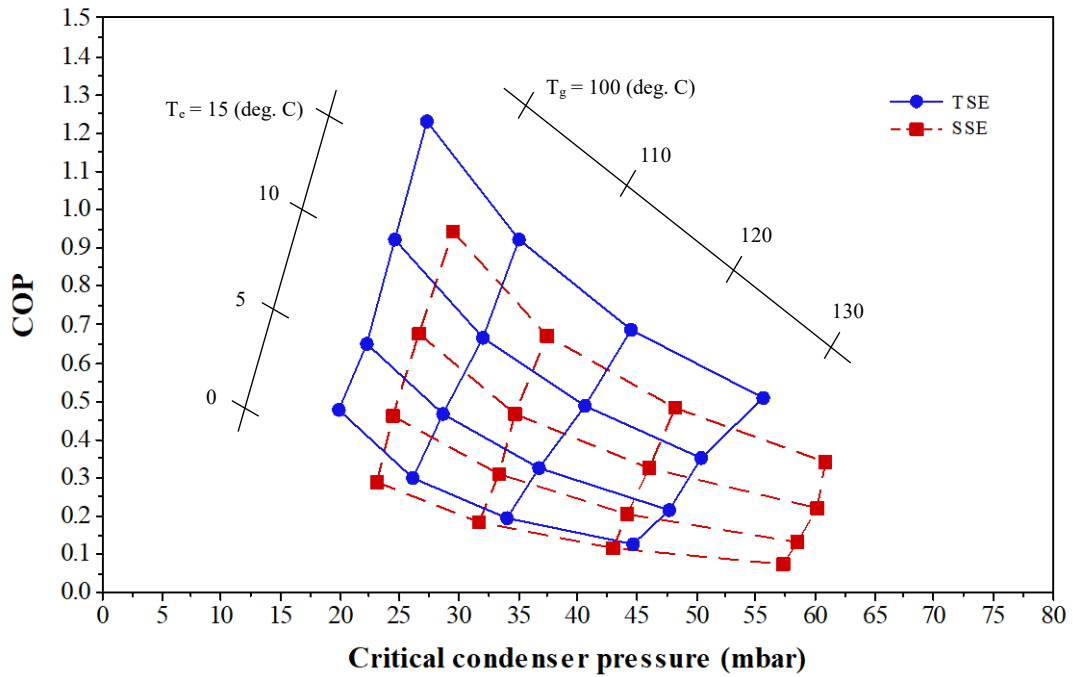


**Figure 4.10 Refrigeration capacity map**

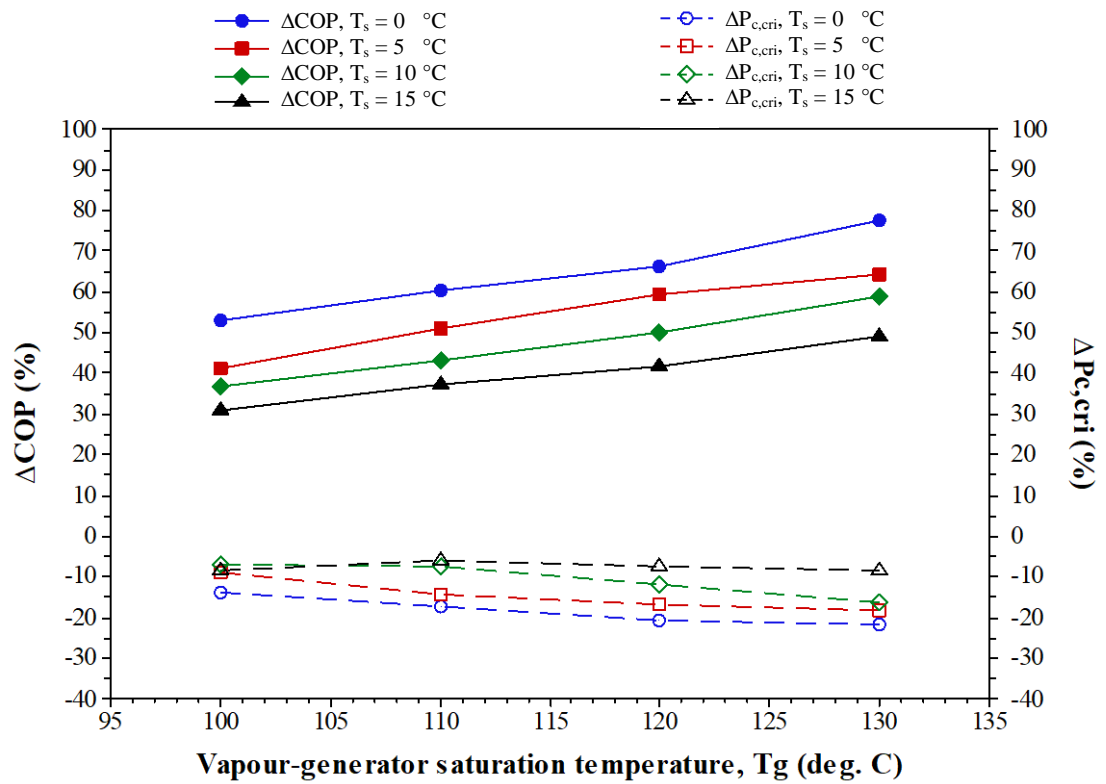


**Figure 4.11 Demonstrates difference percentage of COP, and critical condenser pressure ( $P_{c,cri}$ ) between TSE and SSE**

In summary, the TSE gave much better performance for the entrainment ratio, but the critical back pressure was slightly lower. There is a high potential to employ in the real system. To further improve the TSE, the TSE refrigeration system should use the check valve in the secondary fluid inlet (stage 2), as shown in Figure 4.12. This check valve is the key element in the prevention of reversed flow to the secondary flow inlet and preventing the circumstance of malfunctions or failure of the TSE refrigeration system practically.

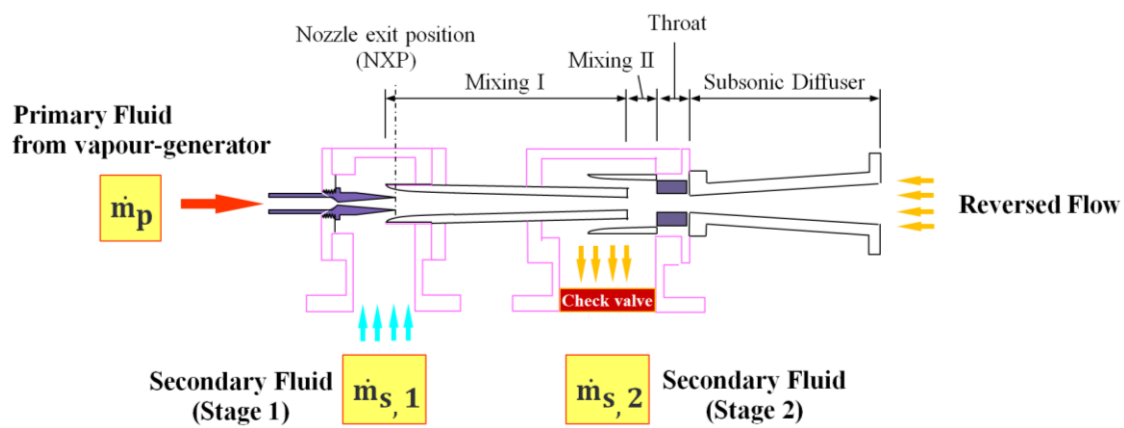


**Figure 4.12 Schematic view of two-stage ejector**

Figure 4.13 shows the validation of secondary fluid mass flow rate of SSE and TSE refrigeration system where the TSE had the check valve in the secondary fluid inlet at the second stage when the primary fluid temperature was at 110 °C and secondary fluid temperature was at 10 °C. As a result, the maximum secondary fluid mass flow rate of SSE was 0.0012793 kg/s, and the maximum critical condenser pressure was 34.64 mbar (26.5 °C). The maximum secondary fluid mass flow rate of TSE for each mixing chamber at the first stage ( $\dot{m}_{s,1}$ ) was 0.0010724 kg/s and maximum critical condenser pressure was 35.67 mbar (27.0 °C), and mixing chamber at the second stage ( $\dot{m}_{s,2}$ ) was 0.0007541 kg/s, and maximum critical condenser pressure was 32.07 mbar (25.2 °C). The sum of secondary mass flow rate represented by TSE at the first stage ( $\dot{m}_{s,1}$ ), and the second stage ( $\dot{m}_{s,2}$ ) was 0.0018265 kg/s which was significantly higher than the SSE induction.

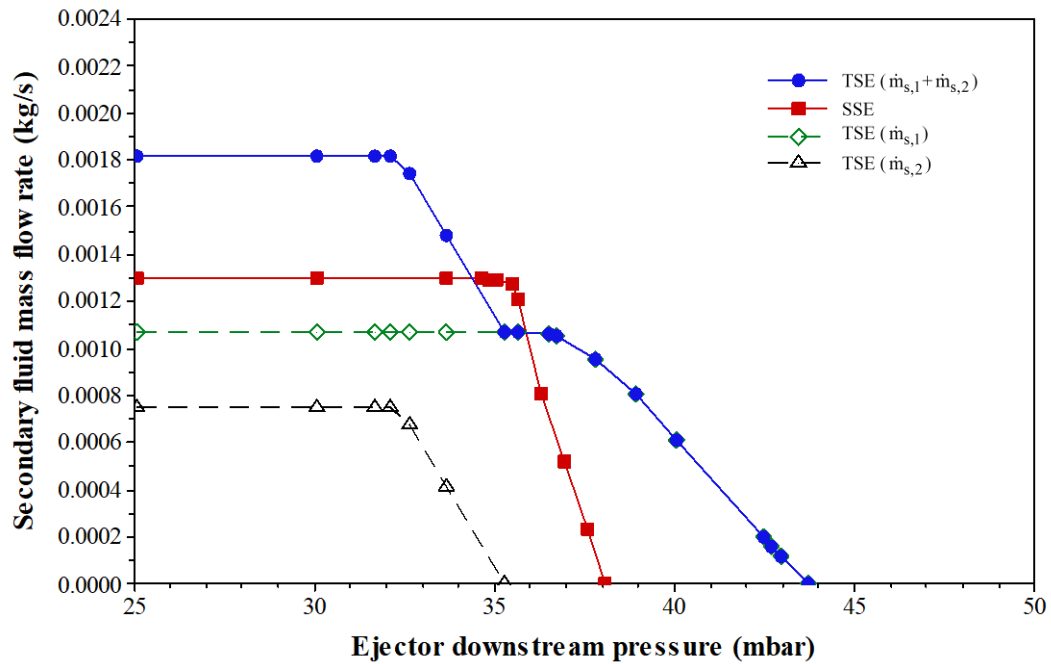


**Figure 4.13 Validation of secondary fluid mass flow rate of SSE, and TSE has to the check valve in the secondary fluid inlet (stage 2)**

Comparison of CFD results between the secondary mass flow rate of SSE and TSE were under these operating conditions: the area ratio ( $A_4/A_6$ ) of 1.6, the length ( $L_4$ ) of  $2.0D_4$ , and the convergence angle ( $\theta_{II}$ ) of  $4^\circ$ . The generator temperature was  $110^\circ\text{C}$ , and the evaporator temperature was at  $0$  and  $15^\circ\text{C}$ , as shown in Figure 4.14 and Figure 4.15, respectively. The evaporator temperature was  $10^\circ\text{C}$  and the generator temperature was at  $100^\circ\text{C}$  and  $120^\circ\text{C}$ , as shown in Figure 4.16 and Figure 4.17, respectively.

The validated Rm of SSE and TSE steam ejector at the generator temperature of  $100$ ,  $110$ , and  $120^\circ\text{C}$  with the evaporator temperature of  $10^\circ\text{C}$  are shown in Figure 4.18. The Rm comparison of SSE and TSE on the refrigeration system at the evaporator temperature of  $0$ ,  $5$ , and  $10^\circ\text{C}$  with the generator temperature of  $110^\circ\text{C}$  are shown in Figure 4.19. The comparison of Rm in terms of the effect of operating conditions are shown in Figure 4.20. The calculated entrainment ratio could be found in Table A.1 at Appendix A.

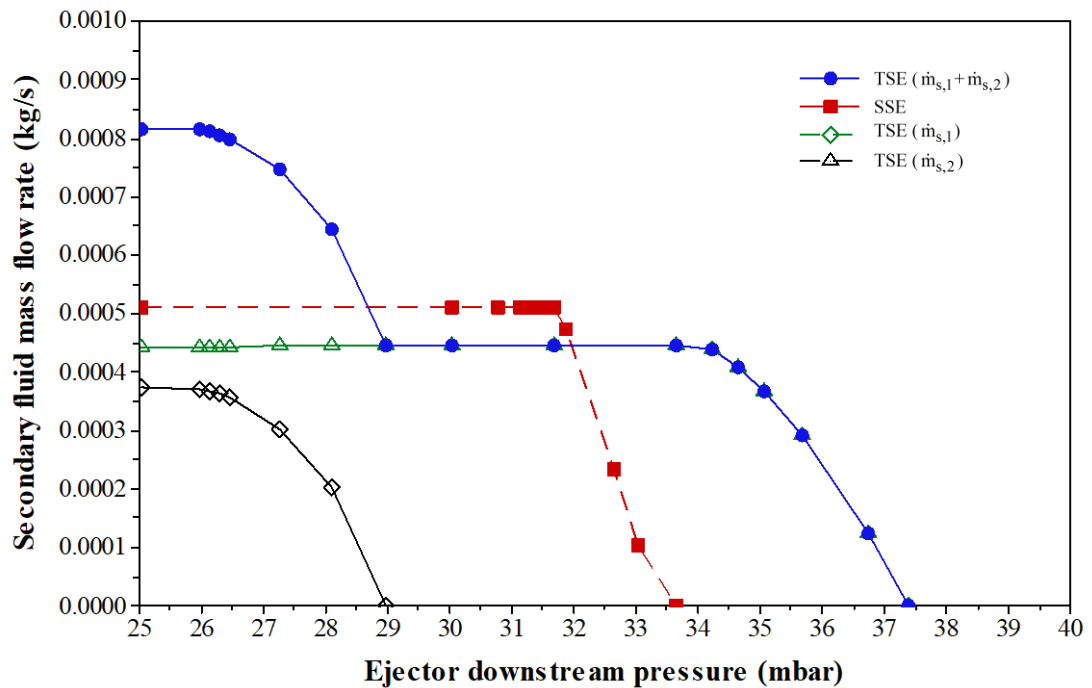


**Figure 4.14** Secondary fluid mass flow rate of SSE and TSE steam ejector at the generator temperature of 110 °C, evaporator temperature of 0 °C

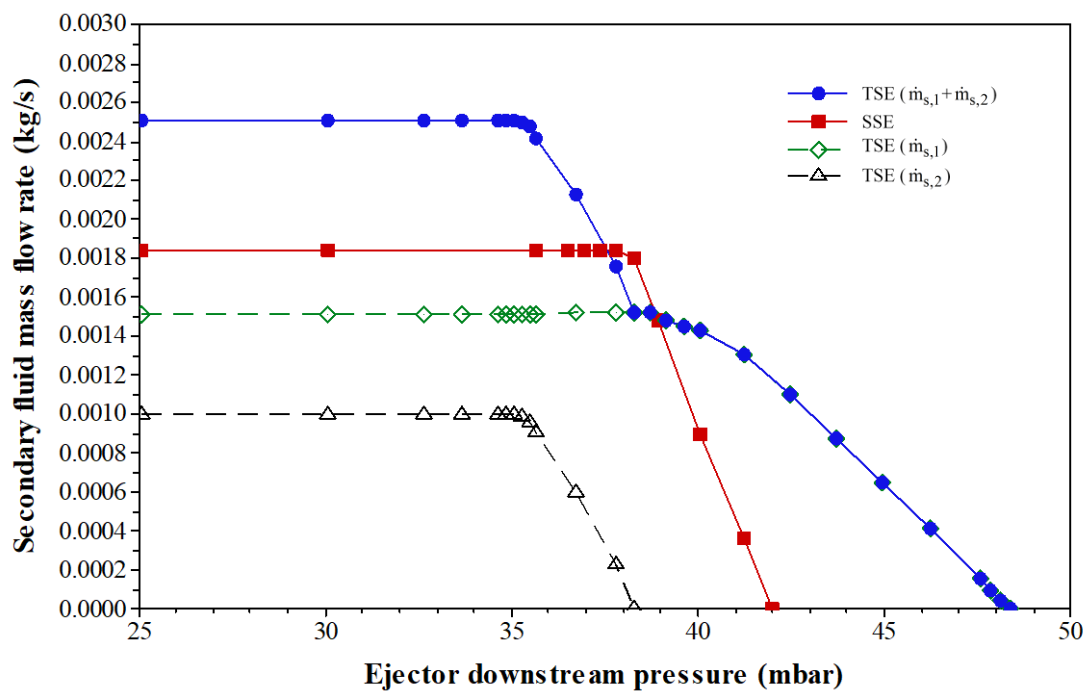


**Figure 4.15** Secondary fluid mass flow rate of SSE and TSE steam ejector at the generator temperature of 110 °C, evaporator temperature of 15 °C

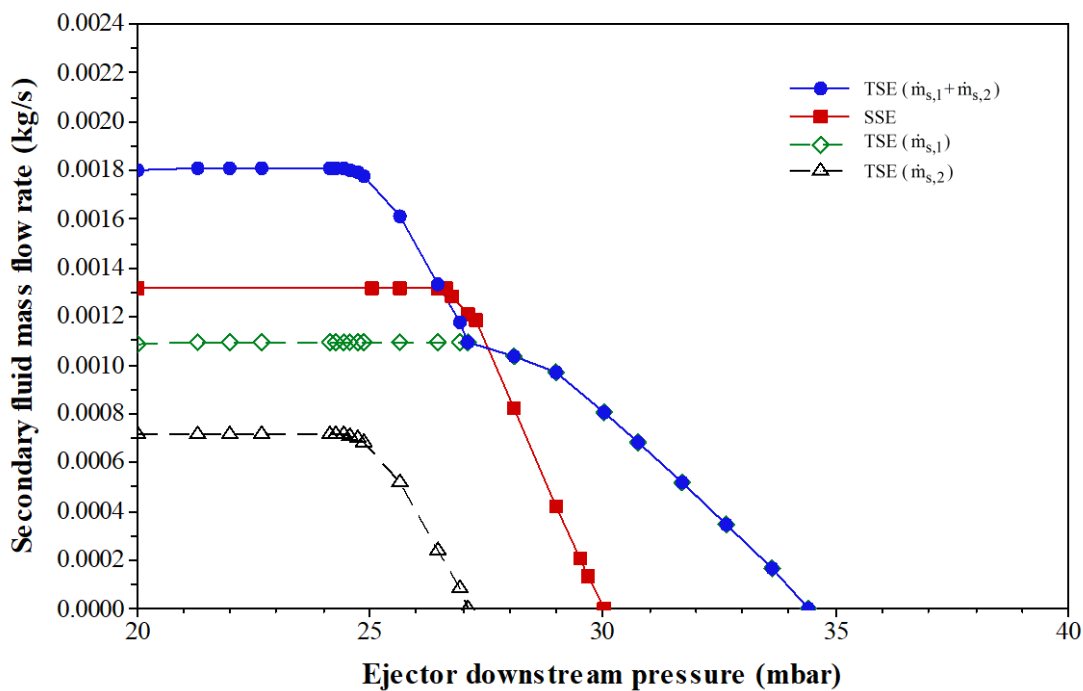


**Figure 4.16** Secondary fluid mass flow rate of SSE and TSE steam ejector at the generator temperature of 100 °C, evaporator temperature of 10 °C

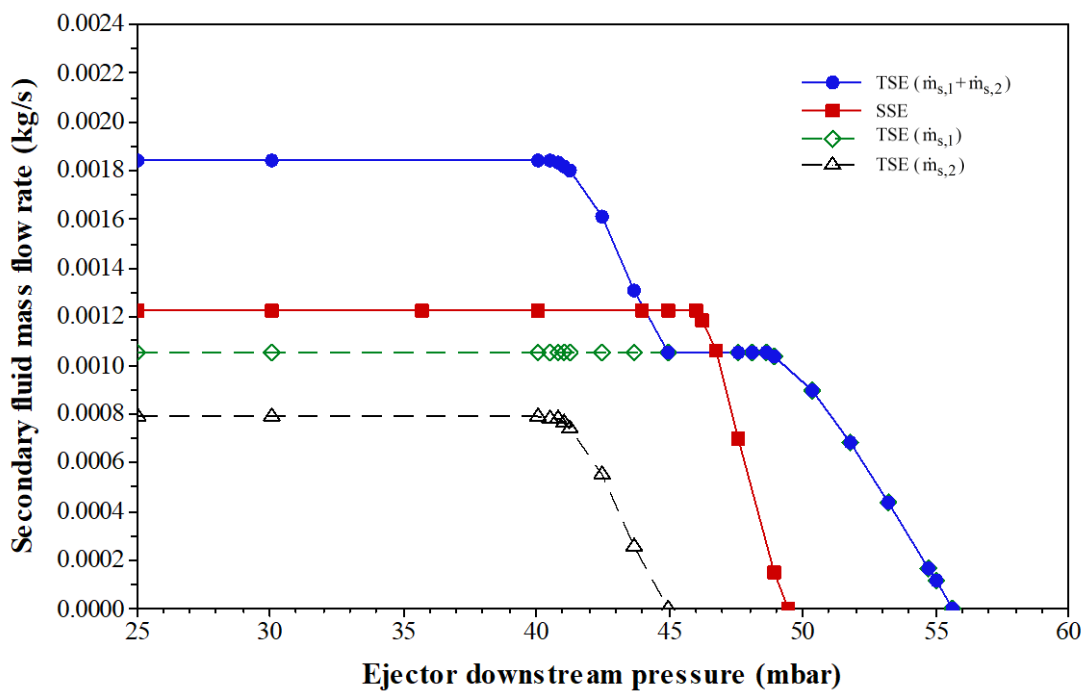


**Figure 4.17** Secondary fluid mass flow rate of SSE and TSE steam ejector at the generator temperature of 120 °C, evaporator temperature of 10 °C

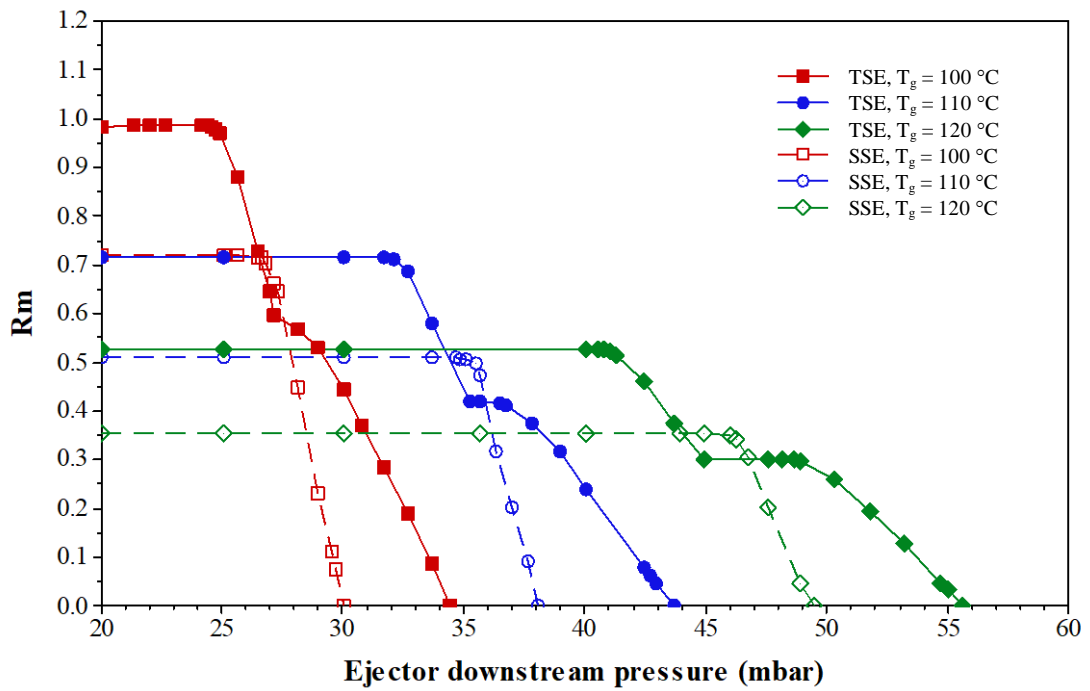


**Figure 4.18** The Rm of SSE and TSE steam ejector at the generator temperature of 100, 110, and 120 °C, evaporator temperature of 10 °C

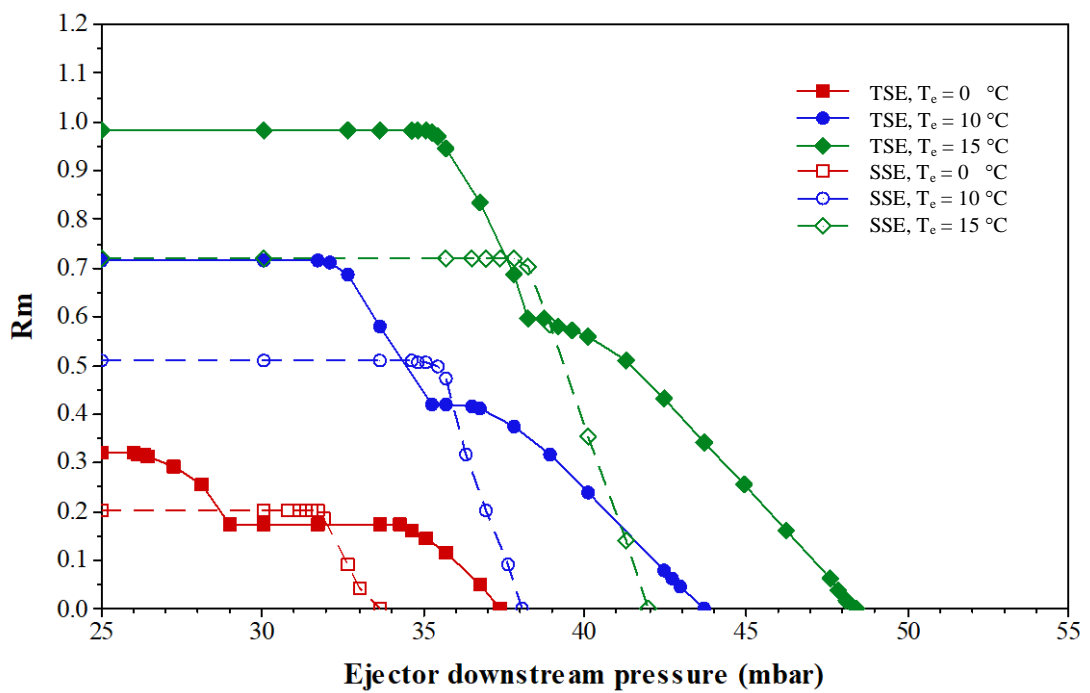


**Figure 4.19** The Rm of SSE and TSE steam ejector at the generator temperature of 110 °C, evaporator temperature of 0, 10, and 15 °C

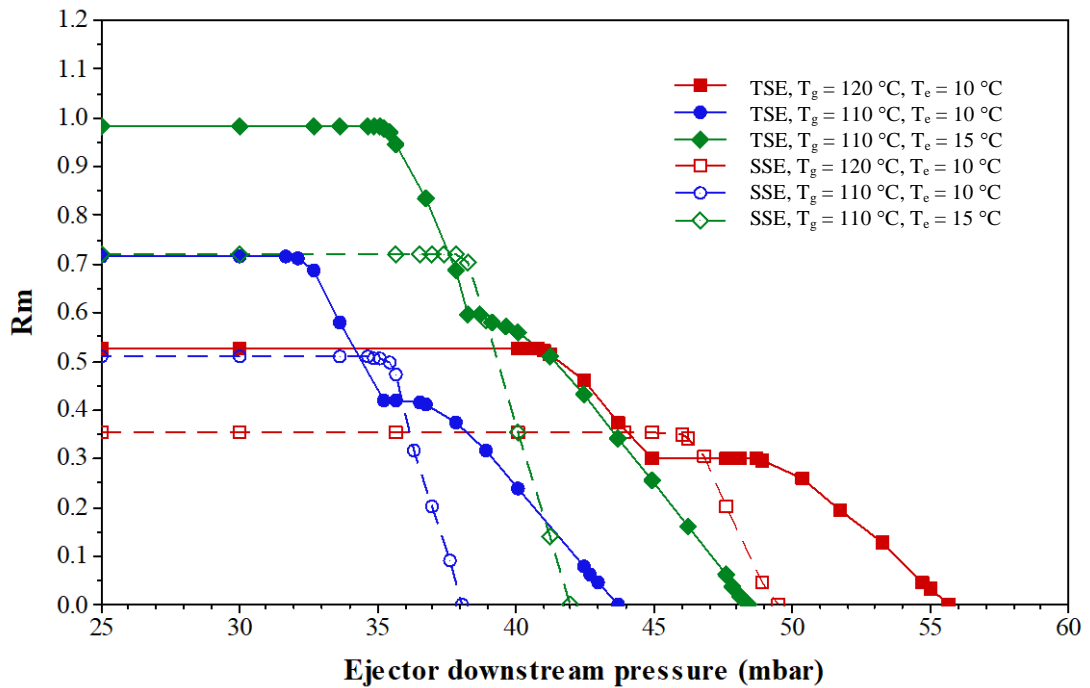


**Figure 4.20** The Rm of SSE and TSE steam ejector at the generator temperature of 110 and 120 °C, evaporator temperature of 10 and 15 °C

## 4.2 CFD and experimental of gas/gas ejector system

The CFD results of the gas/gas ejector system model were validated with the experimental data.

### 4.2.1 CFD results data

The CFD in the gas/gas ejector system results were compared between the Rm of SSE and TSE under the operating conditions from the previous work. The effect of the primary inlet pressure ( $P_p$ ) and the secondary inlet pressure are shown in Figure 4.21 and Figure 4.22, respectively. The Rm of SSE and TSE gas/gas ejector at the secondary inlet pressures were between 0.0 and 1.0 bar which are shown in Figure 4.22. Performance characteristics of the gas/gas ejector validated at the primary inlet pressures of 4 and 5 bar are shown in Figure 4.23 and 4.24, respectively. The SSE and TSE of validated the Rm according to the effect of operating conditions are shown in Figure 4.25.

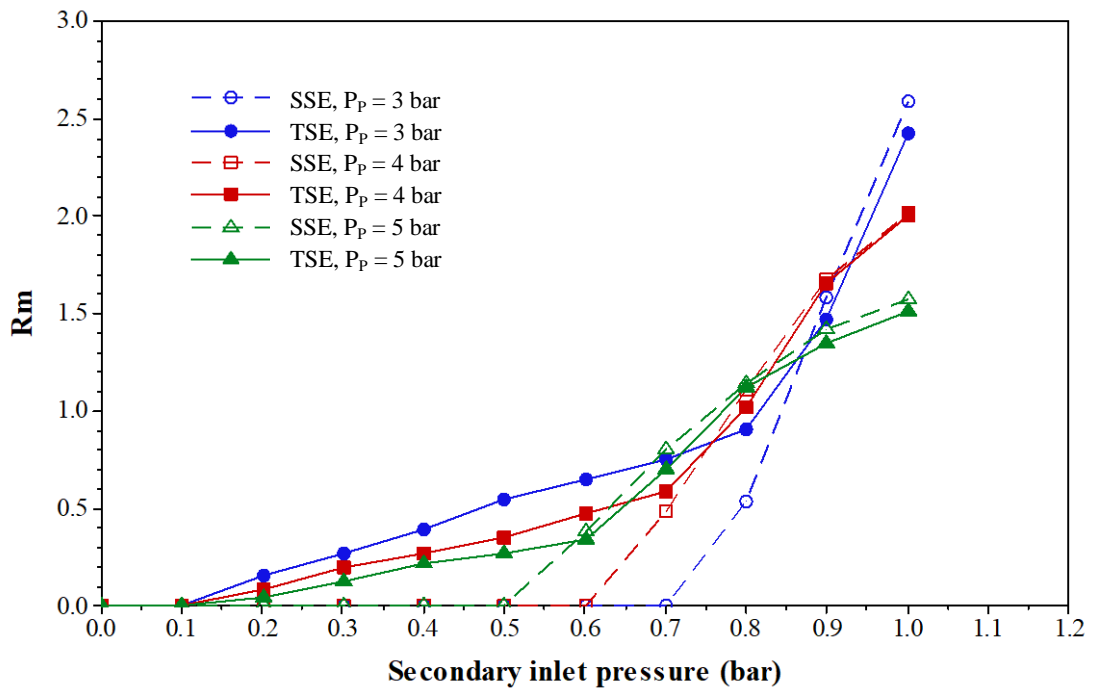


Figure 4.21 Rm of SSE and TSE gas/gas ejector at the secondary inlet pressures are between 0.0 and 1.0 bar

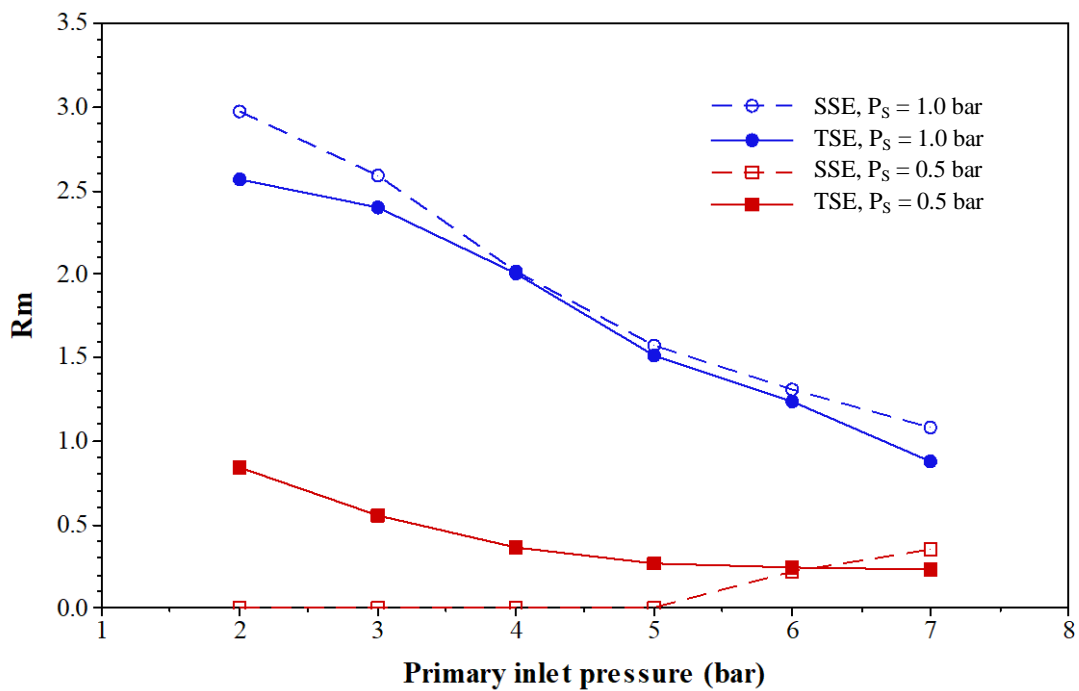
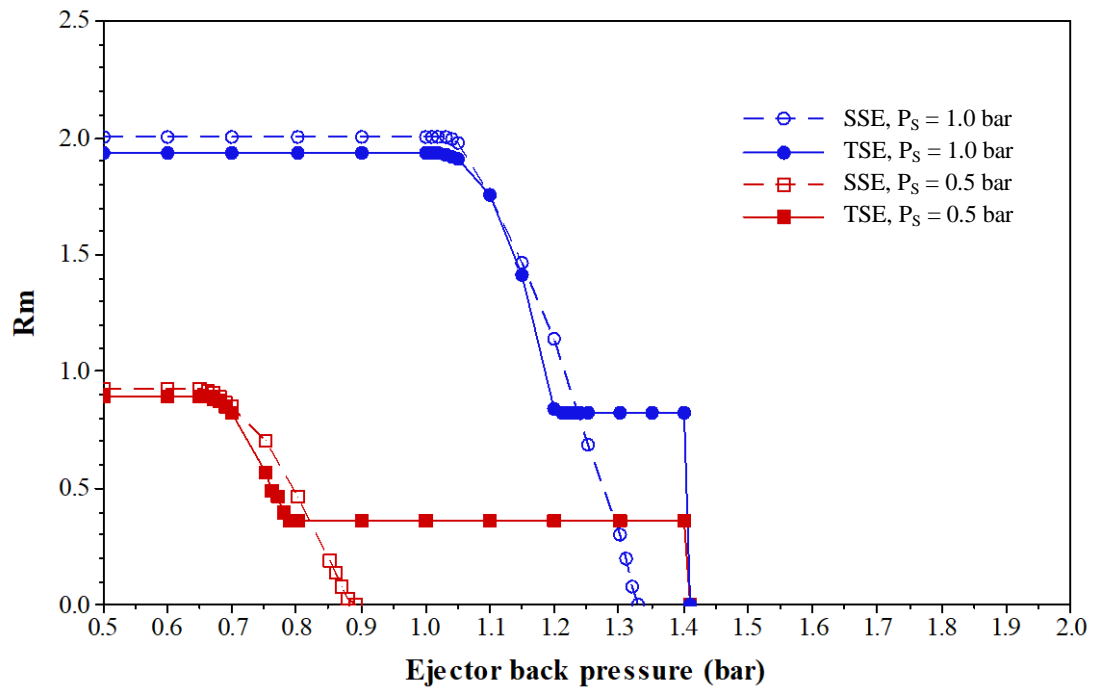
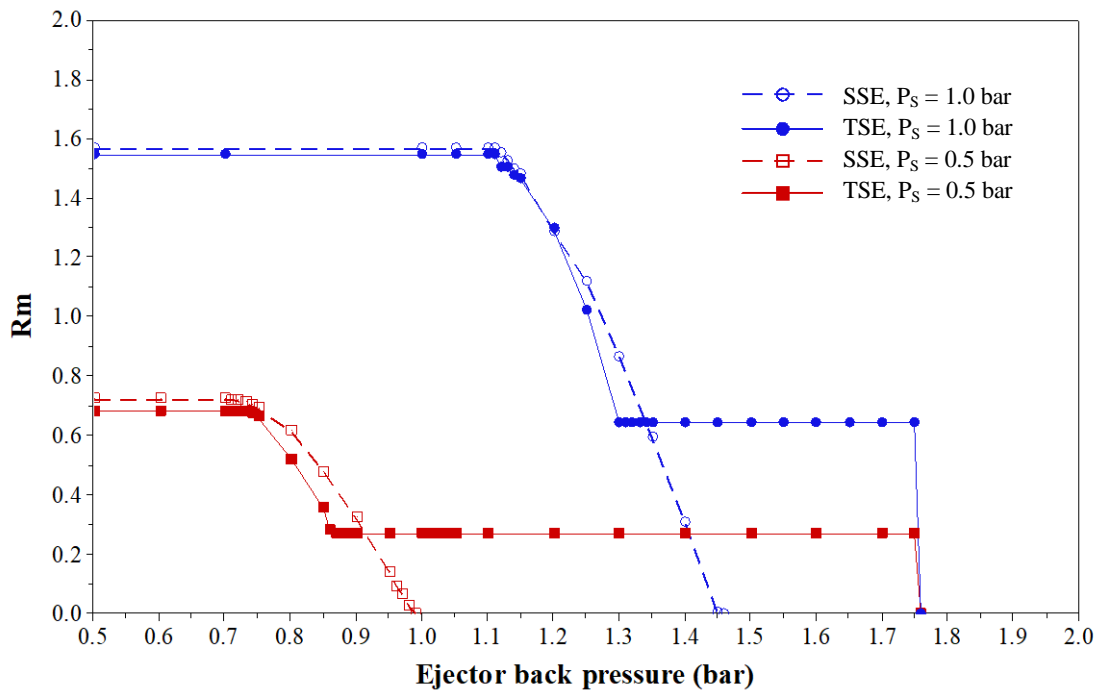


Figure 4.22 Rm of SSE and TSE gas/gas ejector at the primary inlet pressures are between 2 and 7 bar



**Figure 4.23** Performance characteristics of the gas/gas ejector  
at the primary inlet pressures is 4 bar



**Figure 4.24** Performance characteristics of the gas/gas ejector  
at the primary inlet pressures is 5 bar

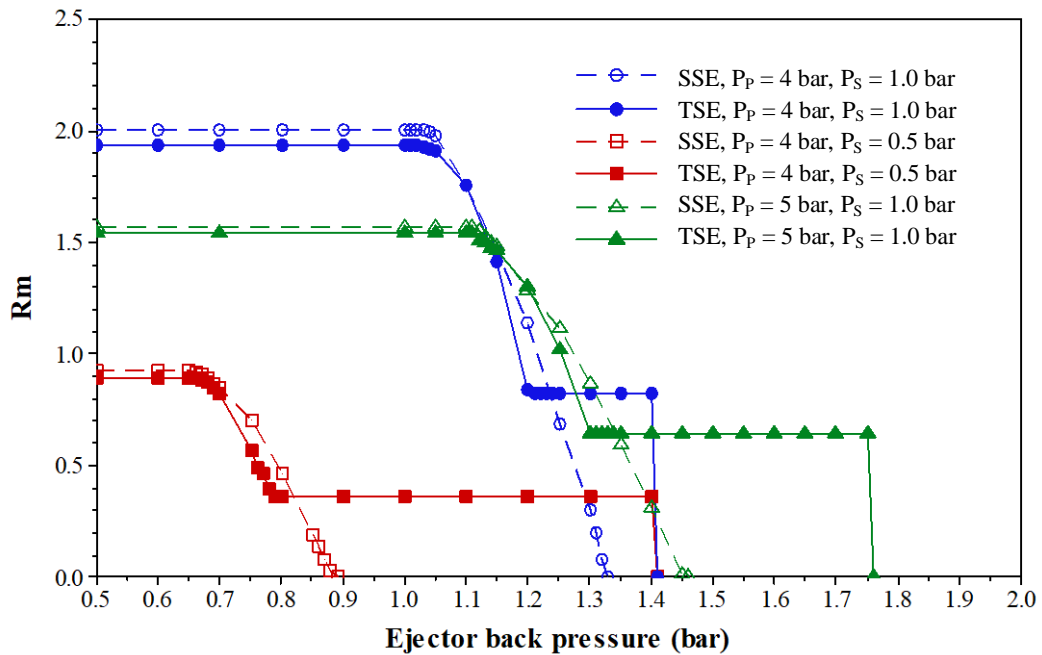
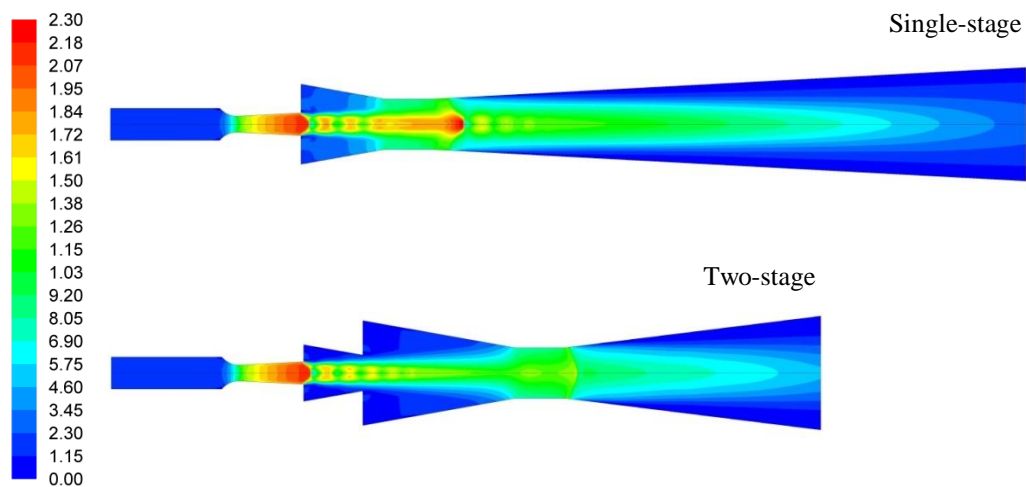


**Figure 4.25 Validation of  $R_m$ , effect of operating conditions.**

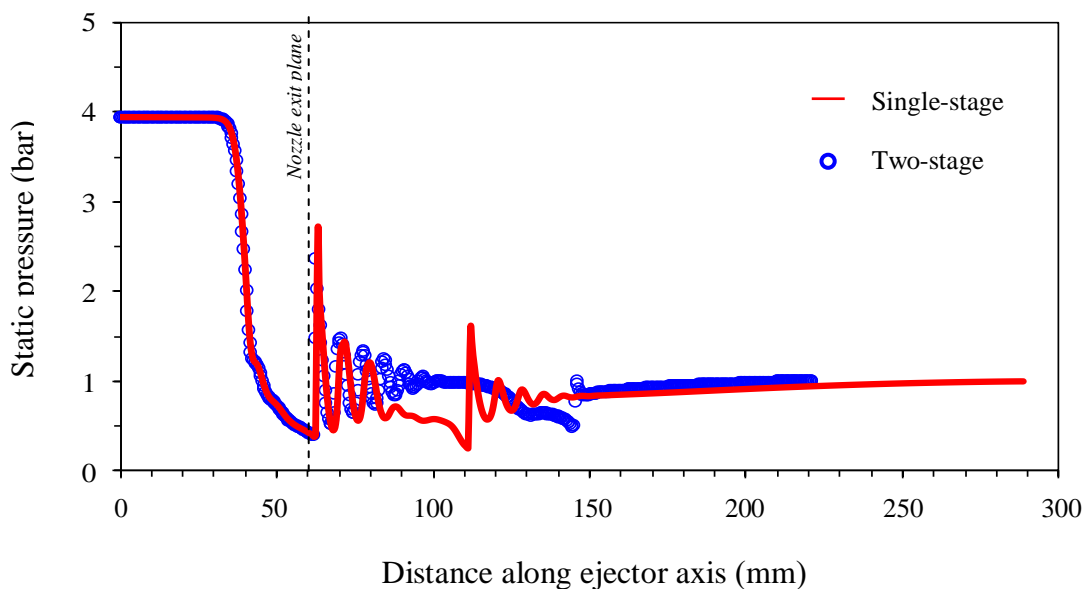
Figure 4.26 shows the simulation results investigation on the performance of the gas/gas ejector system using a two-stage ejector compared with a single-stage ejector.

Figure 4.26(a) shows the contours of Mach number of the ejector comparing between single-stage ejector and two-stage ejector. The primary inlet pressure, secondary inlet pressure, and outlet pressure were 4 bar, 1 bar, and 1 bar, respectively. The single-stage ejector with a larger jet core moves with a slightly greater speed and hence a higher momentum. In a two-stage ejector, better mixing of the secondary fluid causes the smaller one.

Figure 4.26(b) shows the static pressure profiles along the axis of both ejectors. The two-stage ejector has a lower shock to the outlet allowing more secondary flow to be induced.



(a) Filled contours of Mach number



(b) Static pressure distribution along the centerline of the ejector

**Figure 4.26 Comparison advantages of two-stage ejector and single-stage ejector in the gas/gas system**

#### 4.2.2 Validation of the primary fluid mass flow rate

The primary flow rates predicted by CFD were mostly over predicted compared to the measurement values. The comparison between CFD and the experimental results, when the primary inlet pressure was 4 bar to 5 bar, showed the primary flow rate error of 2.61%, and 3.00%, respectively. The primary flow rate average error was 2.805%, as shown in Table 4.1.

**Table 4.1 Validation of calculated primary mass flow rate with the experimental values**

$P_p$ (bar)	Primary mass flow rate, $\dot{m}_p$			
	CFD (kg/s)	CFD ( $m^3/h$ )	Experiment ( $m^3/h$ )	Error (%)
4	0.01814	54.42	53	2.61
5	0.02268	68.04	66	3.00
Average error (%)				2.805

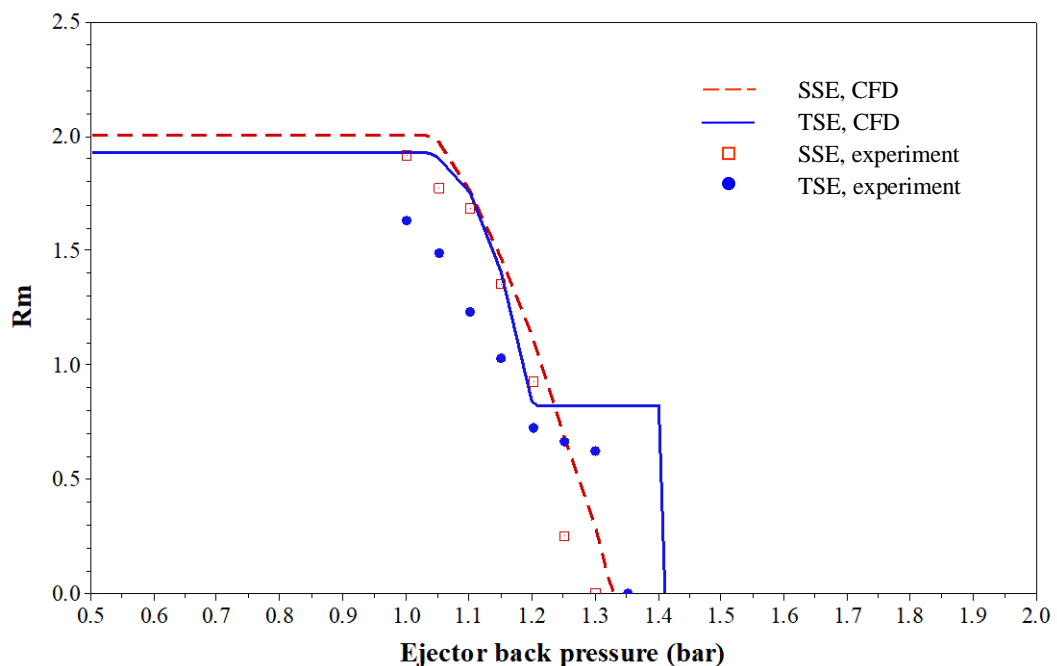
#### 4.2.3 Validation of the entrainment ratio and critical back pressure

The ejector performance characteristic validated between calculation by CFD and the experimental values, when the operating conditions on the primary pressure inlet was between 4 to 5 bar and secondary pressure inlet was between 0.9 to 1 bar in the gas/gas ejector system, are shown in Figure 4.27, Figure 4.28, and Figure 4.29.

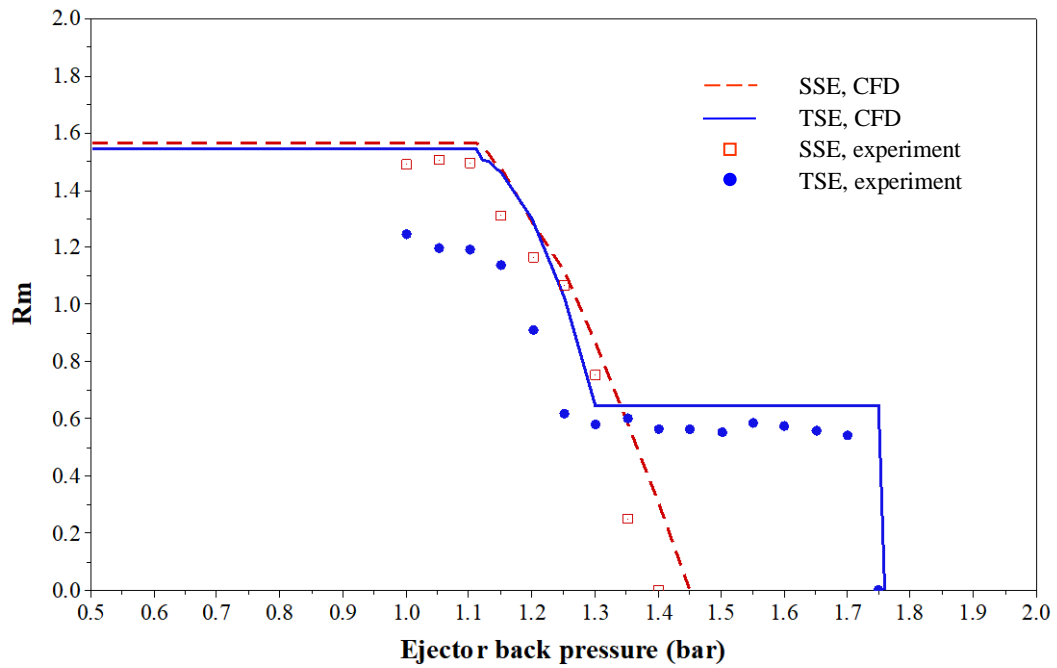
Figure 4.27 shows the TSE performance in the gas/gas ejector system compared with the SSE simulations using CFD that when the primary inlet pressure is 4 bar, the secondary inlet pressure is 1 bar. The TSE provides a marginal decrease entrainment ratio of 3.73% but increases critical back pressure of 35.92%. It was found that the predicted performances of the CFD simulated models agreed well with the experimental values. Average errors of the predicted entrainment ratio and the critical back pressure were 18.54% and 2.00%, respectively.

Figure 4.28 shows the TSE performance in the gas/gas ejector system compared with the SSE simulations using CFD that when the primary inlet pressure is 5 bar, the secondary inlet pressure is 1 bar. The TSE provides a marginal decrease entrainment ratio of 1.40% but increases critical back pressure of 57.66%. It was found that the predicted performances of the CFD simulated models agreed well with the experimental values. Average errors of the predicted entrainment ratio and the critical back pressure were 24.44% and 5.71%, respectively.

Figure 4.29 shows the TSE performance in the gas/gas ejector system compared with the SSE simulations using CFD that when the primary inlet pressure is 5 bar, the secondary inlet pressure is 0.9 bar. The TSE provides a marginal decrease entrainment ratio of 5.02% but increases critical back pressure of 69.90%. It was found that the predicted performances of the CFD simulated models agreed well with the experimental values. Average errors of the predicted entrainment ratio and the critical back pressure were 17.70% and 3.00%, respectively.



**Figure 4.27 Validation of performance characteristics between the SSE and the TSE at  $P_p = 4$  bar and  $P_s = 1$  bar**



**Figure 4.28** Validation of performance characteristics between the SSE and the TSE at  $P_p = 5$  bar and  $P_s = 1$  bar

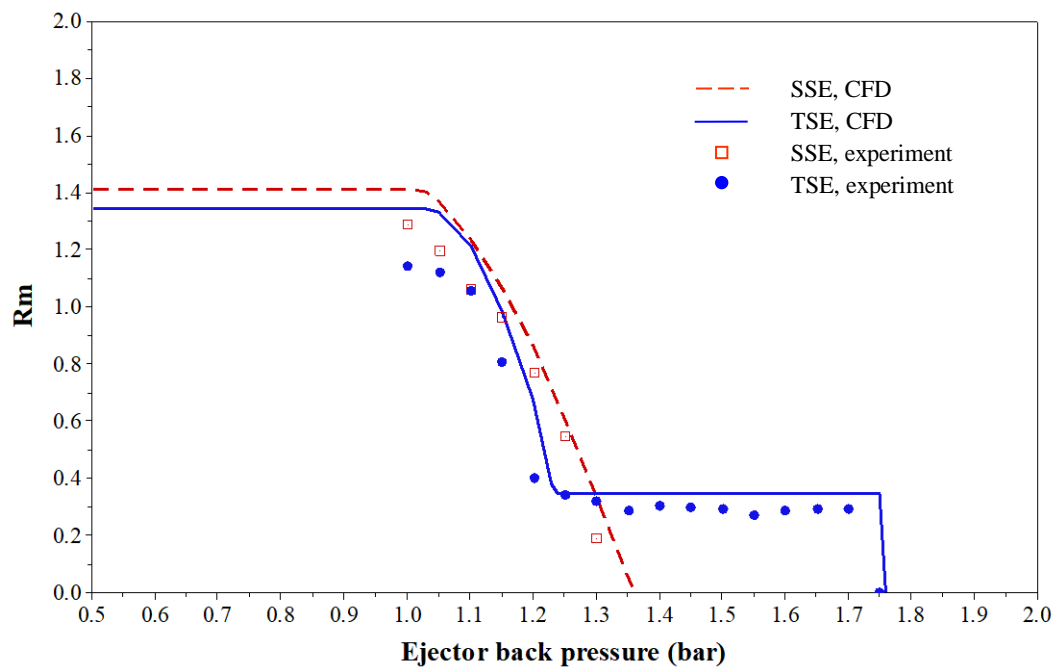


**Figure 4.29** Validation of performance characteristics between the SSE and the TSE at  $P_p = 5$  bar and  $P_s = 0.9$  bar

#### 4.2.4 Validation of the wall static pressure distributions

The CFD validation of the wall static pressure distributions with the experimental data, when the operating conditions on the primary pressure inlet was between 4 to 5 bar and secondary pressure inlet was between 0.9 to 1 bar in the gas/gas ejector system, are shown in Figure 4.30, Figure 4.31, and Figure 4.32. The static pressures along the wall of the ejector were measured of 10-port on the TSE, and 15-port on the SSE.

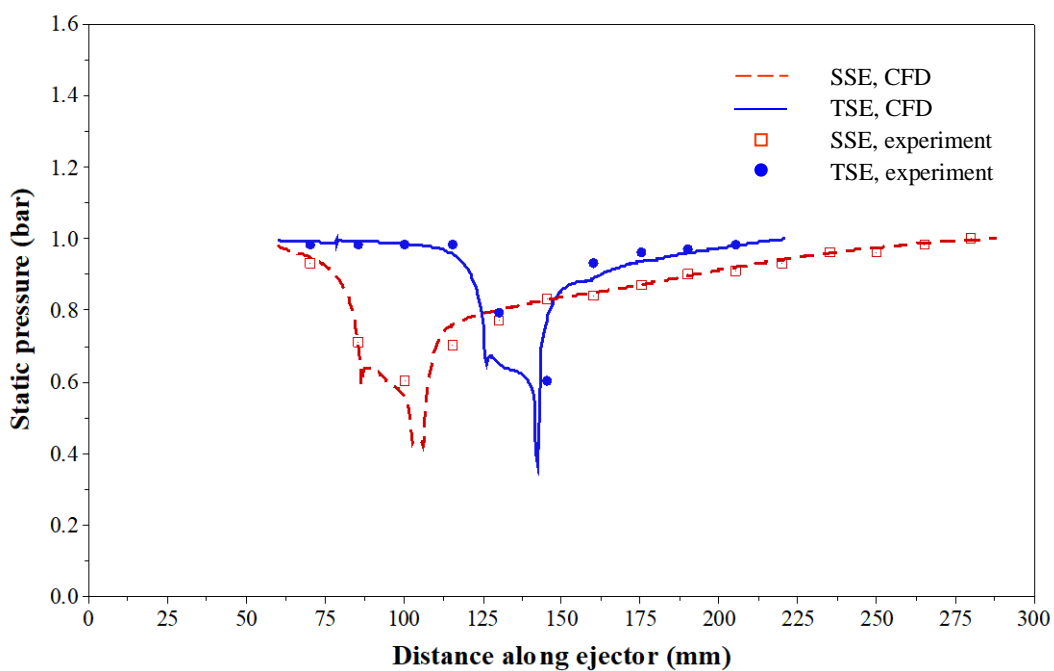


**Figure 4.30** Validation of static pressure profile along ejector between the SSE and the TSE at  $P_P = 4$  bar and  $P_S = 1$  bar

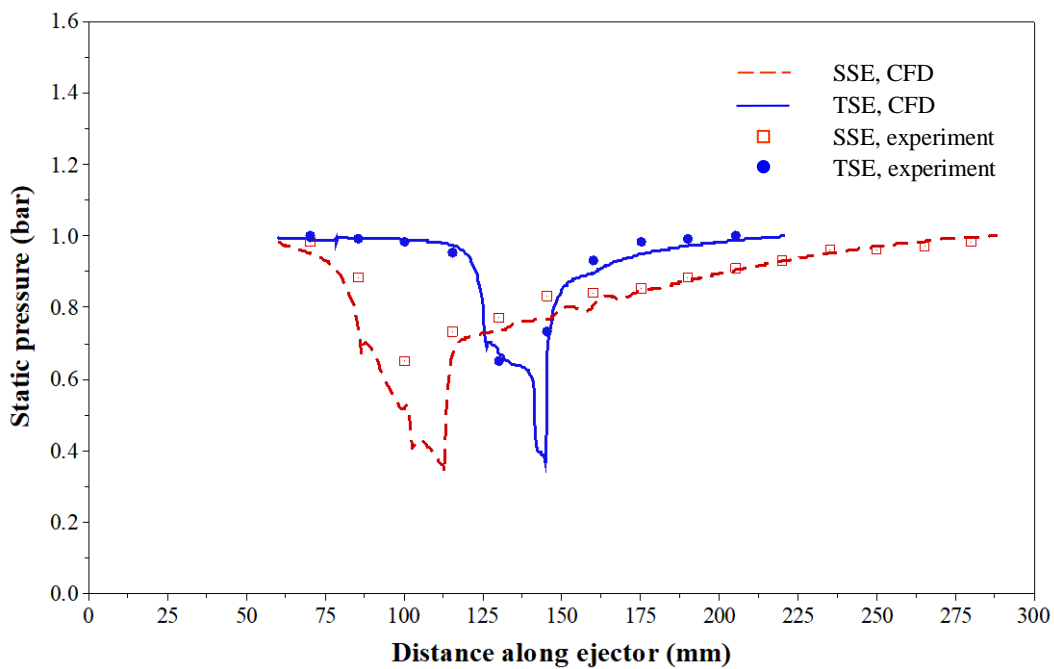


**Figure 4.31** Validation of static pressure profile along ejector between the SSE and the TSE at  $P_P = 5$  bar and  $P_S = 1$  bar

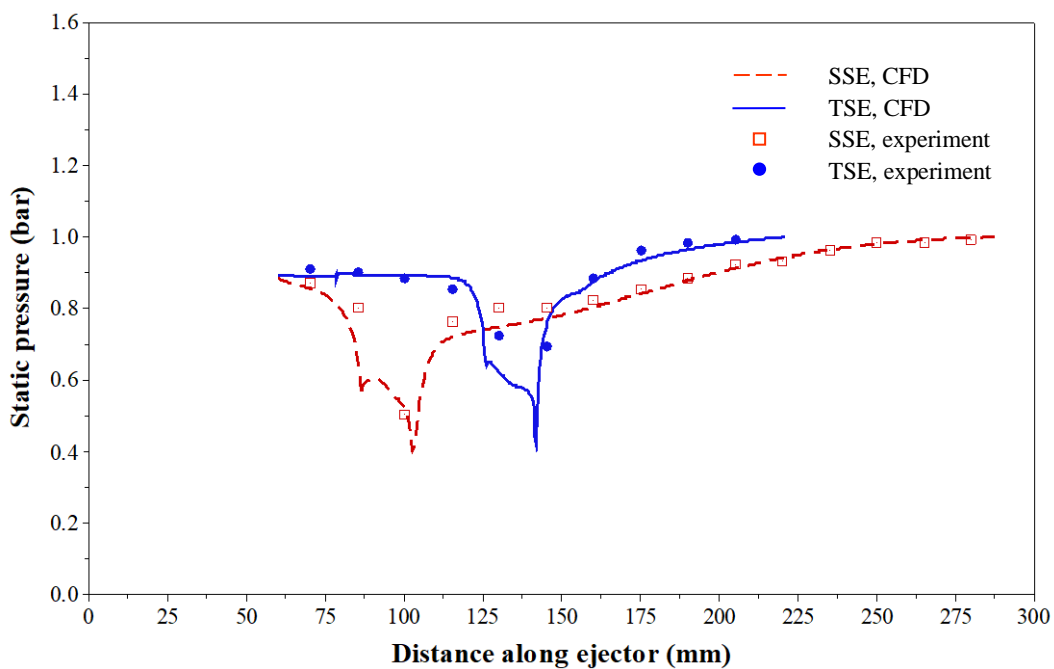


**Figure 4.32** Validation of static pressure profile along ejector between the SSE and the TSE at  $P_P = 5$  bar and  $P_S = 0.9$  bar

After the achievement in validating the simulated results with the experimental values, it can be said that the CFD study in this research was just one of the efficient utilizing methods. The comparison between the CFD analysis and the experimental results of the ejector's performance in terms of  $R_m$  and CBP for the TSE and the SSE are also illustrated in Table B.1 at Appendix B.

## CHAPTER 5

### CONCLUSIONS AND RECOMMENDATIONS

#### 5.1 Conclusions

This thesis studied the design of the proposed two-stage ejector (TSE) type annular secondary at the second stage without changing the area ratio ( $A_r$ ) of the ejector to investigate the performance of ejector refrigeration system and the gas/gas ejector application using the validation of the computational fluid dynamics (CFD) and experimental results compared with the single-stage ejector (SSE).

In the simulation, the TSE performances were investigated by using the various-operating conditions in the steam ejector refrigeration system compared with the single-stage ejector (SSE). For the optimum geometry of TSE, the area ratio ( $A_4/A_6$ ) was 1.6, the length ( $L_4$ ) was  $2.0D_4$ , and the convergence angle ( $\theta_{II}$ ) was  $4^\circ$ . The TSE was investigated by adopting the operating conditions from the previous work whose generator temperatures were between  $100^\circ\text{C}$  and  $130^\circ\text{C}$ , and the evaporator temperatures were between  $0^\circ\text{C}$  and  $15^\circ\text{C}$ . The TSE provided a higher entrainment ratio by up to 77.2%, while there was a marginal decrease in critical back pressure up to the maximum value of 21.9%. It can be concluded that the TSE greatly benefited the refrigeration system, which needs high refrigerating capacity while the condensing pressure was slightly subsided.

Furthermore, the study of the TSE performance in the gas/gas ejector system compared with the SSE simulations using CFD showed that when the primary inlet pressure was 4 bar and secondary inlet pressure was 1 bar. The TSE provided a marginal decrease entrainment ratio of 3.73% but increased critical back pressure of 35.92%. It was found that the predicted performance of the CFD simulated models were agreed well with the experimental values. Average errors of the predicted entrainment ratio and the critical back pressure were 18.54% and 2.00%, respectively.

In conclusion, the TSE which increased in critical back pressure can improve the ejector performance in terms of the entrainment ratio ( $R_m$ ) during the choked flow. The findings of this study can contribute toward advanced fields of ejector

refrigeration. The TSE gave similar performance characteristics curve of a steam ejector, at each setting of primary fluid from vapour-generator and secondary fluid from evaporator condition, the operation of the ejector refrigeration can be categorized into 3 regions: the choked flow, the unchoked flow and the reversed flow of secondary fluid. In practice, the TSE refrigeration system is suggested to have the check valve in the secondary fluid inlet at the second stage. This can improve the ejector performance in terms of entrainment ratio ( $R_m$ ) on the choked flow, downstream an ejector pressure, and break down pressure on the unchoked flow (i.e. reversed flow).

## **5.2 Recommendations**

The CFD study of the two-stage ejector in this research helped in terms of accuracy of the model facility to be more efficient comparing experimental data with computer simulated data. It would still be useful to understand more about the flow phenomena in the TSE. Although the model did not involve the real gas, equations should be applied. An important area of future improvement in TSE refrigeration system studies should be the relationship between its geometries and a specified level of the  $R_m$  and the CBP which are more realistic. Other substitute refrigerants that could be used in a simulation and also in an experiment should also be investigated.

## **REFERENCES**

## REFERENCES

- [1] Chen, J. and et al. “A review on versatile ejector applications in refrigeration systems”, **Renewable and Sustainable Energy Reviews**. 49: 67-90; September, 2015.
- [2] Besagni, G., Mereu, R., and Inzoli, F. (2016). “Ejector refrigeration: A comprehensive review”, **Renewable and Sustainable Energy Reviews**. 53: 373-407; January, 2016.
- [3] Grazzini, G. and Mariani, A. “A simple program to design a multi-stage jet-pump for refrigeration cycles”, **Energy Conversion and Management**. 39(16): 1827-1834; November, 1998.
- [4] Grazzini, G. and Rocchetti, A. “Numerical optimization of a two-stage ejector refrigeration plant”, **International Journal of Refrigeration**. 25(5): 621-633; August, 2002.
- [5] Kong, F. and Kim, H.D. “Analytical and computational studies on the performance of a two-stage ejector-diffuser system”, **International Journal of heat and mass transfer**. 85: 71-87; June, 2015.
- [6] Kong, F. and Kim, H.D. “Optimization study of a two-stage ejector-diffuser system”, **International Journal of heat and mass transfer**. 101: 71-87; October, 2016.
- [7] Gosney, W.B. **Principle of refrigeration**. Cambridge: Cambridge University Press, 1982.
- [8] Keenan, J.H. and Neumann, E.P. “A simple air ejector”, **ASME Journal of Applied Mechanics**. 64: 75-82, 1942.
- [9] Keenan, J.H. Neumann, E.P. and Lustwerk, F. “An investigation of ejector design by analysis and experiment”, **ASME Journal Applied Mechanics**. 17: 299-309, 1950.
- [10] Chunnanond, K. and Aphornratana, S. “Ejectors: applications in refrigeration technology”, **Renewable and Sustainable Energy Reviews**. 8(2): 129-155; April, 2004.

**REFERENCES (CONTINUED)**

- [11] Eames, I.W. Aphornratana, S. and Haider, H. “A theoretical and experimental study of a small-scale steam jet refrigerator”, **International Journal of Refrigeration**. 18(6): 378-386; July, 1995.
- [12] ESDU – Engineering Sciences Data Unit. **Ejector and Jet Pump Design for Steam Driven Flow (Item No.86030)**. London: s.n.,1986.
- [13] ASHRAE. “Steam-jet refrigeration equipment”, in **ASHRAE Guide and Data Book**. US: ASHRAE, 1969.
- [14] Stoecker, W.F. **Refrigeration and Air Conditioning**. New York: McGraw-Hill, 1959.
- [15] Chunnanond, K. and Aphornratana, S. “An experimental investigation of a steam ejector refrigerator: the analysis of the pressure profile along the ejector”, **Applied Thermal Engineering**. 24(2-3): 311-322; February, 2004.
- [16] He, S. Li, Y. and Wang, R.Z. “Progress of mathematical modeling on ejector”, **Renewable and Sustainable Energy Reviews**. 13(8): 1760-1780; October, 2009.
- [17] He, S. Li, Y. and Wang, R.Z. “A new approach to performance analysis of ejector refrigeration system using grey system theory”, **Applied Thermal Engineering**. 29(8-9): 1592-1597; June, 2009.
- [18] Huang, B.J. and et al. “A 1-D analysis of ejector performance”, **International Journal of Refrigeration**. 22(5): 354-364; August, 1999.
- [19] Sriveerakul, T. Aphornratana, S. and Chunnanond, K. “Performance prediction of steam ejector using computational fluid dynamic: Part 1. Validation of the CFD results”, **International Journal of Thermal Sciences**. 46(8): 812-822; August, 2007.
- [20] Zhu, X. and Jiang, P. “Experimental and numerical investigation of the effect of shock wave characteristics on the performance”, **International Journal of Refrigeration**. 40: 31-42; April, 2014.

**REFERENCES (CONTINUED)**

- [21] Aphornratana, S. and Eames, I.W. “A small capacity steam-ejector refrigerator: experimental investigation of a system using ejector with movable primary nozzle”, **International Journal of Refrigeration**. 20(5): 352-358; August 1997.
- [22] Sriveerakul, T., Aphornratana, S., and Chunnanond, K. “Performance prediction of steam ejector using computational fluid dynamic: Part 2. Flow structure of a steam ejector influenced by operating pressure and geometries”, **International Journal of Thermal Sciences**. 46(8): 823-833; August, 2007.
- [23] Zhu, Y. and et al. “Numerical investigation of geometry parameters for design of high performance ejector”, **Applied Thermal Engineering**. 29(5-6): 898-905; April, 2009.
- [24] Ma, X. and et al. “Performance testing of a novel ejector refrigerator for various controlled conditions”, **International Journal of Energy Research**. 35(14): 1229-1235; November, 2011.
- [25] Pereira, P.R. and et al. “Experimental results with a variable geometry ejector using R600a as working fluid”, **International Journal of Refrigeration**. 46: 77-85; October, 2014.
- [26] Ariaifar, K. and et al. “Ejector primary nozzle steam condensation: Area ratio effects and mixing layer development”, **Applied Thermal Engineering**. 71(1): 519-527; October, 2014.
- [27] Varga, S. and et al. “Experimental and numerical analysis of a variable area ratio steam ejector”, **International Journal of Refrigeration**. 34(7): 1668-1675; November, 2011.
- [28] Yapici, R. and et al. “Experimental determination of the optimum performance of ejector refrigeration system depending on ejector area ratio”, **International Journal of Refrigeration**. 31(7): 1183-1189; November, 2008.

**REFERENCES (CONTINUED)**

- [29] Gramisans, X. Sarra, M. and Lafuente, F.J. “Gas pollutants removal in a single- and two-stage ejector–venture scrubber”, **Journal of Hazardous Materials**. 90(3): 251-266; March, 2002.
- [30] Yu, J. Song, X. and Ma, M. “Theoretical study on a novel R32 refrigeration cycle with a two-stage suction ejector”, **International Journal of Refrigeration**. 36(1): 166-172; January, 2013.
- [31] Chen, W.X. and et al. “Numerical assessment on the performance of two-stage ejector to boost the low-pressure natural gas”, **Journal of Natural Gas Science and Engineering**. 34: 575-584; August, 2016.
- [32] Chen, G. and et al. “Performance analysis of a two-stage mechanical compression-ejector cooling cycle intended for micro-trigeneration system”, **International Journal of Refrigeration**. 81: 33-40; September, 2017.
- [33] Hwang, J.J. “Passive hydrogen recovery schemes using a vacuum ejector in a proton exchange membrane fuel cell system”, **Journal of Power Sources**. 247: 256-263; February, 2014.
- [34] Hwang, J.J. and et al. “Numerical and experimental investigation into passive hydrogen recovery scheme using vacuum ejector”, **Journal of Power Sources**. 275: 539-546; February, 2015.
- [35] Abdulateef, J.M. and et al. “Review on solar-driven ejector refrigeration technologies”, **Renewable and Sustainable Energy Reviews**. 13(6-7): 1338-1349; August-September, 2009.
- [36] Zhang, W. and et al. “Optimum selection of solar collectors for a solar-driven ejector air conditioning system by experimental and simulation study”, **Energy Conversion and Management**. 63: 106-111; November, 2012.
- [37] Omidvar, A., and et al. “Entropy analysis of a solar-driven variable geometry ejector using computational fluid dynamics”, **Energy Conversion and Management**. 119: 435-443; July, 2016.
- [38] Allouche, Y. and et al. “Dynamic simulation of an integrated solar-driven ejector based air conditioning system with PCM cold storage”, **Applied Energy**. 190: 600-611; March, 2017.

## REFERENCES (CONTINUED)

- [39] Zegenhagen, M.T., and Ziegler, F. “Feasibility analysis of an exhaust gas waste heat driven jet-ejector cooling system for charge air cooling of turbocharged gasoline engines”, **Applied Energy**. 160: 221-230; December, 2015.
- [40] Strušnik, D. and et al. “Energy efficiency analysis of steam ejector and electric vacuum pump for a turbine condenser air extraction system based on supervised machine learning modeling”, **Applied Energy**. 173: 386-405; July, 2016.
- [41] Keerlatiyadatanapat, N. and et al. “Experimental and theoretical investigation of a hybrid compressor and ejector refrigeration system for automotive air conditioning application”, **Engineering Journal**. 21(5): 105-123; September, 2017.
- [42] Huttunen, M. and et al. “Specific energy consumption of cake dewatering with vacuum filters”, **Minerals Engineering**. 100: 144-154; January, 2017.
- [43] Chen, J. and et al. “A review on versatile ejector applications in refrigeration systems”, **Renewable and Sustainable Energy Reviews**. 49: 67-90; September, 2015.
- [44] Besagni, G., Mereu, R., and Inzoli, F. “Ejector refrigeration: A comprehensive review”, **Renewable and Sustainable Energy Reviews**. 53: 373-407; January, 2016.
- [45] Grazzini, G. and Mariani, A. “A simple program to design a multi-stage jet-pump for refrigeration cycles”, **Energy Conversion and Management**. 39(16): 1827-1834; November, 1998.
- [46] Grazzini, G. and Rocchetti, A. “Numerical optimization of a two-stage ejector refrigeration plant”, **International Journal of Refrigeration**. 25(5): 621-633; August, 2002.
- [47] Kong, F. and Kim, H.D. “Analytical and computational studies on the performance of a two-stage ejector-diffuser system”, **International Journal of heat and mass transfer**. 85: 71-87; June, 2015.

**REFERENCES (CONTINUED)**

- [48] Kong, F. and Kim, H.D. “Optimization study of a two-stage ejector-diffuser system”, **International Journal of heat and mass transfer**. 101: 1151-1162; October, 2016.
- [49] Chen, W.X. and et al. “Numerical assessment on the performance of two-stage ejector to boost the low-pressure natural gas”, **Journal of Natural Gas Science and Engineering**. 34: 575-584; August, 2016.
- [50] Sriveerakul, T., Aphornratana, S., and Chunnanond, K. “Performance prediction of steam ejector using computational fluid dynamic: Part 1. Validation of the CFD results”, **International Journal of Thermal Sciences**. 46(8): 812-822; August, 2007.
- [51] ANSYS Inc. **Fluent User’s Guide**. Canonburg, PA. USA: ANSYS Inc, 2012.
- [52] Ruangtrakoon, N. and et al. “CFD simulation on the effect of primary nozzle geometries for a steam ejector in refrigeration cycle”, **International Journal of Thermal Sciences**. 63: 133-145; January, 2013.
- [53] Kolar, J. and Dvorak, V. “Verification of k- $\omega$  SST Turbulence Model for Supersonic Internal Flows”, **World Academy of Science Engineering and Technology International Journal of Mechanical and Mechatronics Engineering**. 5(9): 1715-1719; September, 2011.
- [54] Ruangtrakoon, N. and Aphornratana, S. “Development and performance of steam ejector refrigeration system operated in real application in Thailand”, **International Journal of Refrigeration**. 48: 142-152; December, 2014.
- [55] Pianthong, K. and et al. “Investigation and improvement of ejector refrigeration system using computational fluid dynamics technique”, **Energy Conversion and Management**. 48(9): 2556-2564; September, 2007.

## **APPENDICES**

**APPENDIX A**  
**CFD RESULTS FOR EJECTOR REFRIGERATION SYSTEM**

Table A.1 Comparison of ejector performance from CFD results

Operating Condition (°C)		Entrainment Ratio			Critical Black Pressure (mbar)		
Primary fluid saturated temperature (P <sub>P</sub> )	Secondary fluid saturated temperature (P <sub>S</sub> )	Two-stage ejector (TSE)	Single-stage ejector (SSE)	Difference (%)	Two-stage ejector (TSE)	Single-stage ejector (SSE)	Difference (%)
100	0	0.477	0.312	52.9	19.88	23.10	-13.9
100	5	0.694	0.492	41.1	22.25	24.42	-8.9
100	10	0.981	0.719	36.4	24.75	26.61	-7.0
100	15	1.307	1.000	30.7	27.26	29.79	-8.5
110	0	0.320	0.200	60.0	26.13	31.69	-17.5
110	5	0.503	0.333	51.1	28.62	33.43	-14.4
110	10	0.714	0.500	42.8	32.07	34.64	-7.4
110	15	0.984	0.717	37.2	35.05	37.38	-6.2
120	0	0.209	0.126	65.9	34.04	42.94	-20.7
120	5	0.349	0.219	59.4	36.73	44.19	-16.9
120	10	0.527	0.352	49.7	40.54	45.99	-11.9
120	15	0.736	0.521	41.3	44.44	48.12	-7.6
130	0	0.140	0.079	77.2	44.70	57.21	-21.9
130	5	0.233	0.142	64.1	47.58	58.48	-18.6
130	10	0.378	0.238	58.8	50.33	60.11	-16.3
130	15	0.552	0.371	48.8	55.65	60.80	-8.5
<b>Average</b>				<b>51.1</b>	<b>-12.9</b>		

**Difference (%)** =  $100 \times (\text{CFD's Entrainment Ratio of TSE} - \text{CFD's Entrainment Ratio of SSE}) / \text{CFD's Entrainment Ratio of SSE}$

**APPENDIX B**  
**EXPERIMENTAL AND CFD RESULTS FOR**  
**THE GAS/GAS EJECTOR APPLICATION**

**Table B.1 Experimental and CFD results for the gas/gas ejector application**

Operating Condition (bar)			Entrainment Ratio							
Primary inlet pressure (P <sub>p</sub> )	Secondary inlet pressure (P <sub>s</sub> )	Ejector back pressure (P <sub>b</sub> )	Two-stage ejector (TSE)			Single-stage ejector (SSE)			EXP Difference (%)	CFD Difference (%)
			EXP	CFD	Error (%)	EXP	CFD	Error (%)		
4.0	1.0	1.00	1.629	1.931	18.5	1.912	2.006	4.9	-14.8	-3.7
4.0	1.0	1.05	1.484	1.911	28.8	1.774	2.006	13.1	-16.3	-4.7
4.0	1.0	1.10	1.233	1.751	42.0	1.686	1.758	4.3	-26.9	-0.4
4.0	1.0	1.15	1.025	1.412	37.8	1.352	1.468	8.6	-24.2	-3.8
4.0	1.0	1.20	0.723	0.842	16.5	0.925	1.135	22.7	-21.8	-25.8
4.0	1.0	1.25	0.660	0.865	31.1	0.252	0.685	171.8	161.9	26.3
4.0	1.0	1.30	0.623	0.819	31.5	0.000	0.297	-	-	175.8
4.0	1.0	1.35	0.000	0.819	-	0.000	0.000	-	-	-
4.0	1.0	1.40	0.000	0.000	-	0.000	0.000	-	-	-
5.0	0.9	1.00	1.141	1.343	17.7	1.288	1.414	9.8	-11.4	-5.0
5.0	0.9	1.05	1.121	1.332	18.8	1.197	1.370	14.5	-6.3	-2.8
5.0	0.9	1.10	1.056	1.214	15.0	1.061	1.233	16.2	-0.5	-1.5
5.0	0.9	1.15	0.808	0.988	22.3	0.965	1.066	10.5	-16.3	-7.3
5.0	0.9	1.20	0.399	0.681	70.7	0.768	0.866	12.8	-48.0	-21.4
5.0	0.9	1.25	0.338	0.351	3.8	0.545	0.604	10.8	-38.0	-41.9
5.0	0.9	1.30	0.318	0.351	10.4	0.187	0.338	80.7	70.1	3.8
5.0	0.9	1.35	0.288	0.351	21.9	0.000	0.061	-	-	475.4
5.0	0.9	1.40	0.303	0.351	15.8	0.000	0.000	-	-	-

**Table B.1 Experimental and CFD results for the gas/gas ejector application (continue)**

Operating Condition (bar)			Entrainment Ratio							
Primary inlet pressure (P <sub>p</sub> )	Secondary inlet pressure (P <sub>s</sub> )	Ejector back pressure (P <sub>b</sub> )	Two-stage ejector (TSE)			Single-stage ejector (SSE)			EXP Difference (%)	CFD Difference (%)
			EXP	CFD	Error (%)	EXP	CFD	Error (%)		
5.0	0.9	1.45	0.298	0.351	17.8	0.000	0.000	-	-	-
5.0	0.9	1.50	0.293	0.351	19.8	0.000	0.000	-	-	-
5.0	0.9	1.55	0.273	0.351	28.6	0.000	0.000	-	-	-
5.0	0.9	1.60	0.288	0.351	21.9	0.000	0.000	-	-	-
5.0	0.9	1.65	0.293	0.351	19.8	0.000	0.000	-	-	-
5.0	0.9	1.70	0.293	0.351	19.8	0.000	0.000	-	-	-
5.0	0.9	1.75	0.000	0.000	-	0.000	0.000	-	-	-
5.0	1.0	1.00	1.242	1.545	24.4	1.485	1.567	5.5	-16.4	-1.4
5.0	1.0	1.05	1.192	1.512	26.8	1.500	1.567	4.5	-20.5	-3.5
5.0	1.0	1.10	1.187	1.512	27.4	1.490	1.567	5.2	-20.3	-3.5
5.0	1.0	1.15	1.136	1.464	28.9	1.308	1.480	13.1	-13.1	-1.1
5.0	1.0	1.20	0.909	1.298	42.8	1.162	1.287	10.8	-21.8	0.9
5.0	1.0	1.25	0.616	1.022	65.9	1.066	1.117	4.8	-42.2	-8.5
5.0	1.0	1.30	0.576	0.636	10.4	0.753	0.866	15.0	-23.5	-26.6
5.0	1.0	1.35	0.601	0.645	7.3	0.247	0.595	140.9	143.3	8.4
5.0	1.0	1.40	0.561	0.645	15.0	0.000	0.307	-	-	110.1
5.0	1.0	1.45	0.561	0.645	15.0	0.000	0.000	-	-	-
5.0	1.0	1.50	0.551	0.645	17.1	0.000	0.000	-	-	-

**Table B.1 Experimental and CFD results for the gas/gas ejector application (continue)**

Operating Condition (bar)			Entrainment Ratio							
Primary inlet pressure (P <sub>P</sub> )	Secondary inlet pressure (P <sub>S</sub> )	Ejector back pressure (P <sub>b</sub> )	Two-stage ejector (TSE)			Single-stage ejector (SSE)			EXP Difference (%)	CFD Difference (%)
			EXP	CFD	Error (%)	EXP	CFD	Error (%)		
5.0	1.0	1.55	0.586	0.645	10.1	0.000	0.000	-	-	-
5.0	1.0	1.60	0.571	0.645	13.0	0.000	0.000	-	-	-
5.0	1.0	1.65	0.556	0.645	16.0	0.000	0.000	-	-	-
5.0	1.0	1.70	0.540	0.645	19.4	0.000	0.000	-	-	-
5.0	1.0	1.75	0.000	0.645	-	0.000	0.000	-	-	-
5.0	1.0	1.80	0.000	0.000	-	0.000	0.000	-	-	-

**Error (%)** =  $100 \times (\text{CFD's Entrainment Ratio} - \text{EXP's Entrainment Ratio}) / \text{EXP's Entrainment Ratio}$

**CFD Difference (%)** =  $100 \times (\text{CFD's Entrainment Ratio of TSE} - \text{CFD's Entrainment Ratio of SSE}) / \text{CFD's Entrainment Ratio of SSE}$

**EXP Difference (%)** =  $100 \times (\text{EXP's Entrainment Ratio of TSE} - \text{EXP's Entrainment Ratio of SSE}) / \text{EXP's Entrainment Ratio of SSE}$

## VITAE

**NAME** Mr. Nat Suvarnakuta

**INFORMATION** 111/11 Boongmai, Warinchamrab, Ubon Ratchathani 34190,  
Thailand.

**MAIL ADDRESS** n.suvarnakuta@hotmail.com

**EDUCATION** May 27, 2009 – June 14, 2011  
Master of Engineer (Mechanical Engineering)  
Ubon Ratchathani University, Ubon Ratchathani, Thailand

May 24, 2005 – April 07, 2009  
Bachelor of Engineer (Mechanical Engineering)  
Ubon Ratchathani University, Ubon Ratchathani, Thailand

**EXPERIENCE** July 01, 2017 – present  
UBON RATCHATHANI TECHNICAL COLLEGE  
November 01, 2011 – October 23, 2015  
SURINDRA RAJABHAT UNIVERSITY  
Department of Mechanical Technology, Faculty of Industrial  
Techonlogy, Surindra Rajabhat University  
March 17, 2008 – May 13, 2008